J. Membrane Biol. 98, 169–189 (1987)

The Journal of
Membrane Biology

Potassium-Proton Symport in *Neurospora*: Kinetic Control by pH and Membrane Potential

Michael R. Blatt*, Alonso Rodriguez-Navarro**, and Clifford L. Slayman
Department of Physiology, Yale University School of Medicine, New Haven, Connecticut 06510

Summary. Active transport of potassium in K^+-starved *Neurospora* was previously shown to resemble closely potassium uptake in yeast, *Chlorella*, and higher plants, for which K^+ pumps or K^+/H^+-ATPases had been proposed. For *Neurospora*, however, potassium-proton cotransport was demonstrated to operate, with a coupling ratio of 1 H^+ to 1 K^+ taken inward so that K^+, but not H^+, moves against its electrochemical gradient (Rodriguez-Navarro et al., *J. Gen. Physiol.* **87**:649–674).

In the present experiments, the current-voltage (*I-V*) characteristic of K^+-H^+ cotransport in spherical cells of *Neurospora* has been studied with a voltage-clamp technique, using difference-current methods to dissect it from other ion-transport processes in the *Neurospora* plasma membrane. Addition of 5-200 μM K^+ to the bathing medium causes 10-150 mV depolarization of the unclamped membrane, and yields a sigmoid *I-V* curve with a steep slope (maximal conductance of 10-30 $\mu S/cm^2$) for voltages of −300 to −100 mV, i.e., in the normal physiologic range. Outside that range the apparent *I-V* curve of the K^+-H^+ symport saturates for both hyperpolarization and depolarization. It fails to cross the voltage axis at its predicted reversal potential, however, an effect which can be attributed to failure of the *I-V* difference method under reversing conditions.

In the absence of voltage clamping, inhibitors—such as cyanide or vanadate—which block the primary proton pump in *Neurospora* also promptly inhibit K^+ transport and K^+-H^+ currents. But when voltage clamping is used to offset the depolarizing effects of pump blockade, the inhibitors have no immediate effect on K^+-H^+ currents. Thus, the inhibition of K^+ transport usually observed with these agents reflects the kinetic effect of membrane depolarization rather than any direct chemical action on the cotransport system itself.

Detailed study of the effects of $[K^+]_o$ and pH_o on the *I-V* curve for K^+-H^+ symport has revealed that increasing membrane potential systematically *decreases* the apparent affinity of the transporter for K^+, but *increases* affinity for protons (K_m range: for $[K^+]_o$, 15-45 μM; for $[H^+]_o$, 10-35 nM). This behavior is consistent with two distinct reaction-kinetic models, in which (i) a neutral carrier binds K^+ first and H^+ last in the forward direction of transport, or (ii) a negatively charged carrier (−2) binds H^+ first and K^+ last.

Key Words voltage-dependent cotransport · H^+-K^+ symport · *Neurospora* · current-voltage analysis · ordered-binding models · vanadate inhibition · competitive activation · linear mixed activation · glucose-inhibited transport · fungi

Introduction

Active transport of potassium has similar characteristics in almost all walled eukaryotic cells: dependence on metabolic energy; ability to sustain concentration ratios in the range 10^4–10^5; high-affinity K^+ binding (K_m's near 10 μM); stoichiometric exchange of K^+ for other cations, usually H^+; and activation of these characteristics by K^+ starvation (*see* review in Rodriguez-Navarro, Blatt & Slayman, 1986). There have been two common interpretations of these properties: that they represent operation either of a K^+/H^+ countertransport system (Lin & Hanson, 1976; Barr, Holland & Bower, 1977) or of a cation-exchanging ATPase/pump analogous to the Na^+/K^+-ATPase of animal-cell plasma membranes (Leonard, 1982). Recently, however, Rodriguez-Navarro et al. (1986) have demonstrated, from combined thermodynamic and kinetic evidence, that a system displaying all of these properties in the mycelial fungus *Neurospora* is in fact a K^+-H^+ cotransporter.

The system is elicited by growing cells on limiting K^+ and requires the presence of ca. 100 μM Ca^{2+} in the bathing medium. Its apparent $K_{1/2}$ for potassium is micromolar, but depends on the manner and extent of K^+ depletion (Ramos & Rodriguez-Navarro, 1985). Potassium accumulation via the system is driven by the electrochemical potential difference for protons across the plasma membrane.

* *Present address:* Botany School, University of Cambridge, Cambridge CB2 3EA, U.K.

** *Present address:* Departmento de Microbiologia, Escuela Tecnica Superior de Ingeneeros Agronomos, Cordoba, Spain.

And when operating in parallel with the primary proton-extruding pump in *Neurospora* membranes, the cotransporter *mimics* the postulated K^+/H^+ exchangers. In addition to mediating potassium accumulation by starved cells, the cotransporter can also function to stabilize intracellular pH (pH_i) during acute cytoplasmic acid loading (Blatt & Slayman, 1987).

The present paper constitutes a detailed electrical-kinetic study of the K^+-H^+ symport system in *Neurospora*, directed both toward developing a coherent reaction-kinetic model, and toward answering salient functional questions about the system which have arisen during earlier study (H. Pfrüner & C.L. Slayman, *unpublished experiments;* Rodriguez-Navarro et al., 1986; Rodriguez-Navarro & Ramos, 1986). For example, why—when it is a gradient-driven system—should its normal operation be blocked by general metabolic inhibitors (e.g., cyanide) or even by specific inhibitors of the proton pump (e.g., orthovanadate)? Do changes of pH or membrane potential modulate primarily the limiting velocity of transport, or the affinity of the transport system for the primary substrate (K^+)? Why is the symport system ineffective in concentrating potassium at moderately alkaline pH values (e.g., $pH_o \gtrsim 8$), despite high membrane potentials? Or what is the origin of multiple-K_m influx via the symport, seen under certain conditions in *Neurospora*?

The data have been analyzed in relation to ordered-binding models for mediated transport, and can be quantitatively described by two simple schemes: either a negatively charged "carrier" binds a proton first and then a potassium ion prior to transport, or a neutral "carrier" binds a potassium ion first and then a proton.

Materials and Methods

Growth and Handling of the Cells

Spherical cells of *Neurospora crassa* strain RL21a (wild type) were grown in rotating cultures (25°C, 3 days) from conidia suspended in ammonium phosphate-substituted Vogel's medium (1956), supplemented in 0.3 mM KCl, 1% (wt/vol) glucose, and 15% (vol/vol) ethylene glycol (EG). The cells were harvested and prepared for impalement as described previously (Blatt & Slayman, 1983; Rodriguez-Navarro et al., 1986): after a progressive, 3-hr dilution of EG, the cells were resuspended in a "potassium-free" buffer lacking glucose and then attached to polylysine-treated coverslips which formed the top of the experimental chamber. Individual cells were selected and held for impalement with the aid of a suction pipette, which was withdrawn following successful penetration. A continuous flow of buffer (approx. 10 chamber volumes/min) was maintained in the chamber during the experiments. Bathing solutions were shifted either in the conventional manner, by changing bulk flow through the entire chamber (time-constant for the shift, 5-7 sec), or by means of a movable capillary pipette positioned immediately upstream from the impaled cells (time-constant for the shift, $\lesssim 50$ msec).

Reagents and Solutions

The standard buffer solution for these experiments was 10 mM MES (2-[N-morpholino]ethane sulfonic acid) titrated to pH 5.8 with $Ca(OH)_2$. Flame assays of K^+ contaminating this solution gave 0.5-0.7 μM, which is the real "zero" of $[K^+]_o$ for the experiments reported. The approximate $[Ca^{2+}]$ in the buffer solutions was 1.6 mM. Several other organic buffers were used for selected experiments at different pH values. In most cases, concentrations of approximately 10 mM were titrated with ~1.6 mM $Ca(OH)_2$: ACES (N-[2-acetamido]-2-aminomethane sulfonic acid, pH 6.55); MOPS (morpholinopropane sulfonic acid, pH 6.95); HEPES (N-2-hydroxyethyl piperazine-N-2-ethanesulfonic acid, 7.3); TAPS (3-[2-hydroxy-1,1-bis(hydroxymethyl)ethyl] amino-1-propanesulfonic acid, pH 8.1); and MES (pH 5.2, and pH 6.1). Sugars were omitted from all incubation buffers because carbon starvation is the most effective way to prevent germination (sprouting) of the EG-grown spherical cells; and Na^+ and NH_4^+ were omitted because they interfere with K^+ uptake.

All compounds used were Reagent Grade chemicals obtained either from J.T. Baker Chemical Company (Phillipsburg, NJ), from CalBiochem (American Hoechst Corp., LaJolla, CA), or from Sigma Chemical Company (St. Louis, MO).

Electronics

The recording circuitry described previously (Blatt & Slayman, 1983; Rodriguez-Navarro et al., 1986) was modified to permit rapid *I-V* scanning and interbarrel ionophoresis. The steady-state *I-V* characteristic of the *Neurospora* membrane was determined by a two-electrode method, using a microprocessor both to drive the voltage clamp and to record and analyze the voltage and current data (Gradmann et al., 1978). The voltage was scanned, over the nominal range −400 to +100 mV, by means of a bipolar staircase of 100-msec pulses (24 steps: 12 positive to the stable membrane potential, and 12 negative). A single *I-V* scan required ~5 sec, but this time could be shortened by reducing the number of steps in the clamp cycle. *I-V* scans were normally run immediately preceding, during, and immediately following each potassium treatment or other experimental test.

Interbarrel ionophoresis was used to inject specific ions (H^+, vanadate) into the cells without displacing the membrane potential. For this purpose, two barrels of a 4-barrelled electrode were connected, via 1-M KCl:Ag-AgCl half cells, to two WPI M701 electrometer amplifiers (input impedance 10^{12} Ω, WP Instruments, New Haven, CT). The current inputs of these amplifiers were driven by signals of equal magnitude but opposite sign, generated by the microprocessor. The circuity permitted both ion-holding currents and injection currents up to 500 pA, without affecting the electrical properties of the cell membrane.

Electrode

Two- and four-barreled microelectrodes were manufactured with a modified horizontal puller as described previously (Blatt & Slayman, 1983). The barrels were separated over a small gas

flame and, when filled, were connected in series with their respective electrometer amplifiers via 1-M KCl:Ag-AgCl half-cells. Individual barrels of electrodes tested randomly had resistances of 50-70 MΩ, when filled with 1 M KCl and dipped into the same solution. Both electrode types were free of electrical coupling between barrels, as tested with current pulses of 1 nA amplitude and ~100 μsec rise time. For experiments, electrodes were filled with diluted bridge salt in order to minimize leakage and the subsequent detrimental effects of nonphysiologic cations and anions (Blatt & Slayman, 1983; Rodriguez-Navarro et al., 1986). 50 mM potassium acetate (KOAc) was chosen for most experiments, which had the effect of clamping cytoplasmic potassium, $[K^+]_i$, near 50 mM without introducing the spurious DC conductance due to Cl^- ions (Blatt & Slayman, 1983) or a spasmodic conductance due to SO_4^{2-} (anion action potentials; M.R. Blatt, *unpublished experiments*). In control experiments, prolonged current injections from KOAc-filled pipettes (±100 pA, 30-40 min) had no measureable effect on membrane potentials or *I-V* characteristics of EG-grown cells.

For vanadate injections, one barrel of the microelectrode was filled with 50 mM KOAc plus 5 mM orthovanadate (prepared in a stock solution of 185 mM K_2HVO_4 and 10 mM MES brought to pH ~7.0 with acetic acid). Although the injected vanadate could not be quantified directly under these conditions, the changing membrane *I-V* characteristic, showing inhibition of the proton pump (Bowman & Slayman, 1979; Kuroda et al., 1980; Sanders & Slayman, 1982), served as an indirect assay of intracellular free vanadate.

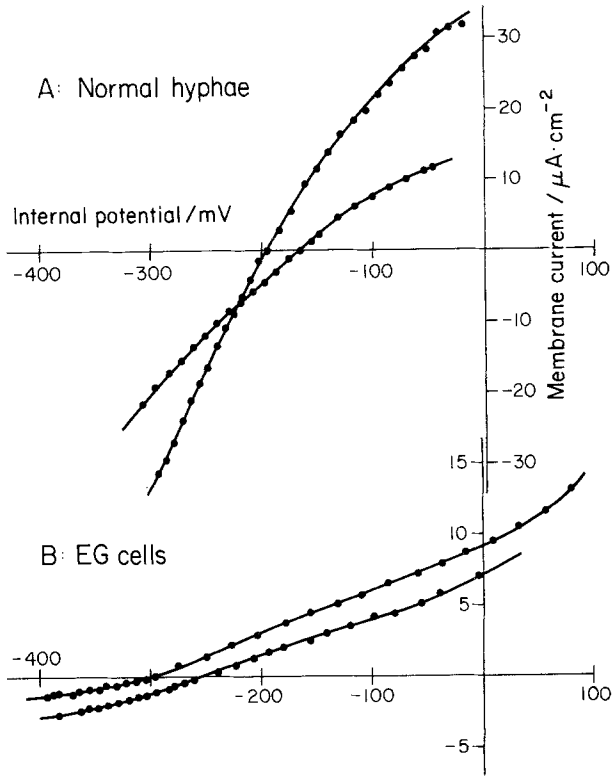

Fig. 1. Typical steady-state membrane current-voltage curves (*I-V* curves) for different cell-types of *Neurospora*. (*A*) Two examples of mature hyphae selected from normal mycelium. Hyphal diameters, 17–20 μm. Grown in Vogel's (1956) minimal medium + 2% sucrose; studied in 20 mM dimethylglutaric acid (buffer) titrated to pH 5.8 with (25 mM) KOH, +1 mM $CaCl_2$ and 1% (wt/vol) glucose. Data from Gradmann et al. (1978), cells W213 and W273. (*B*) Two examples of spherical cells, 13–17 μm diameter, grown on K^+-limited medium containing 15% ethylene glycol; studied in 10 mM MES titrated to pH 5.8, with (1.6 mM) $Ca(OH)_2$ but without added sugar (*see* Materials and Methods). The upper curve is the same as that shown as the control for Fig. 2

Results

General Features of Membrane *I-V* Curves in *Neurospora*

Two examples of the current-voltage characteristic for membranes of normal *Neurospora* hyphae are shown in Fig. 1*A*, and two examples for K^+-starved EG-grown spherical cells are shown in Fig. 1*B*. For hyphal membranes, the curves are generally convex along the positive current axis, sometimes with a single inflection at large negative potentials. The resting membrane potential (V_m) ranges between about −170 and −220 mV (*see* *x* intercepts in Fig. 1*A*), and short-circuit current (I_{sc}) spans 10 to 50 μA/cm² (*see* extrapolated *y* intercepts in Fig. 1*A*). Membrane conductance (G_m) at V_m varies between about 100 and 250 μS/cm², of which approximately 1/2 can be attributed to the electrogenic proton pump and 1/2 to leaks and other electrophoretic pathways (Gradmann et al., 1978; Gradmann, Hansen & Slayman, 1982). Together, the electrophoretic pathways appear nearly linear and can be approximated by a fixed leakage conductance (G_L) and emf (E_L) in series, with $E_L \simeq 0$ mV, so that the leakage current is simply

$$I_L = G_L(V_m - E_L) \simeq G_L V_m. \quad (1)$$

The *I-V* characteristic for membranes of EG-grown *Neurospora* differed in several important ways from that for normal hyphae. It had two inflection points and was concave along the positive current axis, at both large negative and large positive membrane potentials; V_m, −240 to −320 mV in carefully punctured EG-cells, lay beyond the range for hyphae; and membrane conductance at V_m was much lower than in hyphae, 10–50 μS/cm². The rising conductance at strong depolarization persisted when the proton pump was blocked either by cyanide or orthovanadate (*see* Figs. 6 and 8, below). That circumstance, plus the curve's similarity to leakage conductances for potassium ions seen in a variety of plant cells (esp. *Acetabularia*, Gradmann, 1975) and its enhancement by intracellular injection of monovalent cations (M.R. Blatt, *unpublished results*) identifies the rising conductance as a

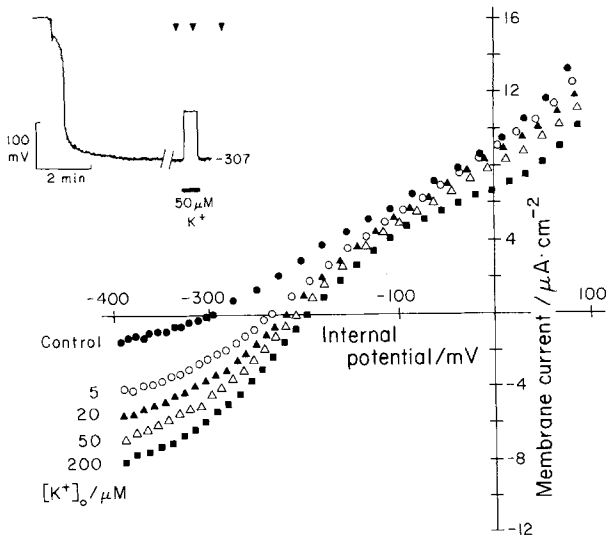

Fig. 2. Influence of added potassium on the steady-state *I-V* curve for a typical low-K spherical cell. *Inset:* Initial part of the voltage recording (with *I-V* scans masked out) to illustrate the time-course of membrane sealing around the electrode and the time-course of depolarization with a brief K^+ pulse. *I-V* scans were made at time indicated by the carats. *Main Diagram: I-V* plots were obtained during sequential K^+ pulses, 5 → 200 μM. Free K^+ concentration for the control curve: < 0.6 μM. The pre- and post-pulse control curves were all very similar, and only one example is shown. Data from the same experiment as in Fig. 5 of Rodriguez et al. (1986)

leakage process, albeit a strongly nonlinear one. On an empirical basis, it could be satisfactorily described by the constant-field relationship (Hodgkin & Katz, 1949). Letting X_i and X_o be the effective intracellular and extracellular concentrations of a putative leakage cation, I_L is written

$$I_L = \frac{F^2V_m}{RT} P_X X_i \frac{1 - (X_o/X_i)\exp(-FV_m/RT)}{1 - \exp(-FV_m/RT)}. \quad (2)$$

Because the responsible ion has not been proven, the apparent concentration ratio X_o/X_i is more meaningful than independent concentrations, and the equation has only two free parameters, P_xX_i and X_o/X_i. Equation (2) can be rearranged into a more convenient form

$$I_L = \frac{F^2V_m}{RT} P_X X_i \frac{1 - \exp(-F(V_m - E_L)/RT)}{1 - \exp(-FV_m/RT)} \quad (3)$$

in which E_L is the diffusion potential for the leakage process.

Comparison of the pairs of *I-V* curves in Fig. 1 makes clear that the proton pump also behaves somewhat differently in EG-grown cells than it does in hyphae. Apart from the difference of scale (pump velocity) referred to above, the pump in EG-cells had slightly different kinetics, but the changes were quantitative rather than fundamental, and will be discussed in a separate paper (D. Sanders, M.R. Blatt, J. Warncke, and C.L. Slayman, *in preparation*). Over most of the important voltage range—for membrane potentials negative to ca. −100 mV—pump (and leak) characteristics could be satisfactorily separated from the behavior of the K^+ transport system by current subtraction.

Apparent Current-Voltage Characteristic for K^+–H^+ Cotransport

A typical time-tracing of membrane potential from K^+-starved spherical cells is shown in Fig. 2 (Inset), along with membrane current-voltage curves obtained upon addition of 5–200 μM $[K^+]_o$. Following penetration of the microelectrode into cells, a period of 20–60 sec was often required for the cell membrane to seal around the electrode. Further experimental manipulations were therefore delayed until both membrane potential and membrane resistance had stabilized. The sealing phenomenon was similar in time course to that reported previously for *Neurospora* hyphae (Slayman, 1965*a*), but the final sealing resistance, $\sim 10^{10}$ Ω, was in the normal range for patch electrodes, rather than the range observed for penetrating electrodes (in hyphae; $<10^9$ Ω). Similar results have been observed on careful penentration of other small, walled cells, such as stomatal guard cells of *Vicia* and *Commelina* (Blatt, 1987). Addition of 50 μM K^+ to the cell bathing medium produced an abrupt ~100-mV depolarization, and removal of the K^+ produced an equally abrupt repolarization. Current-voltage scans, carried out at times indicated by the carats (Fig. 2, Inset), revealed potassium to increase membrane conductance substantially at potentials negative to −100 mV, but to have relatively little effect at potentials positive to −100 mV. Both the magnitude of depolarization (*see* voltage intercepts in Fig. 2) and the voltage-dependence of the conductance change with potassium were concentration dependent, as would be expected for a transported ion (*compare*, e.g., the curves for 5 μM K^+ and for 200 μM K^+, in Fig. 2).

In order to estimate the K^+-induced currents independently of other transport functions in the *Neurospora* membrane, we calculated difference currents (ΔI), by subtracting the control curve (in Fig. 2, for example) from the corresponding K^+ curves, as shown in Fig. 3 (*see* figure legend for technical details). This technique had been used to study a variety of other ion cotransport systems: high-affinity glucose (Hansen & Slayman, 1978) and

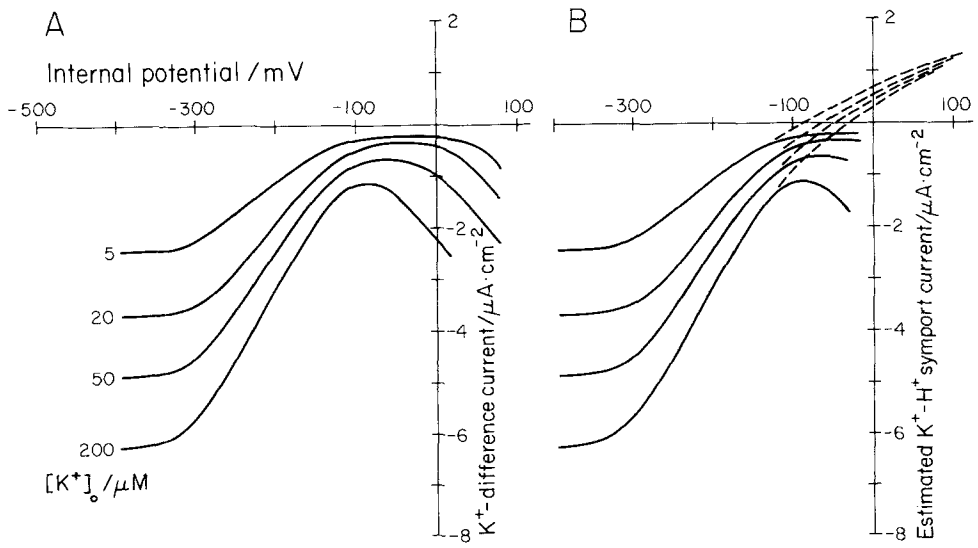

Fig. 3. Difference *I-V* curves (ΔI-V curves) calculated from the experiment of Fig. 2. The bracketing control curves for each K^+ pulse were averaged and subtracted from the experimental curve in Fig. 2. Averaging and subtracting were carried out with polynomial functions (sixth degree) fitted to the *I-V* data points by a nonlinear least-squares algorithm (Marquardt, 1963). (*A*) Actual ΔI-V curves, shown over the full range of clamped voltages. Region of negative slope is an artifact of the subtraction procedure (*see* Results). (*B*) Anticipated actual shape of the *I-V* curves for K^+-H^+ cotransport, obtained by extrapolating (dashed curves) the left-hand portions of ΔI-V curves through the equilibrium potentials estimated for symport (E_{KH}), and extended to a common maximal current at large positive membrane potentials. $[K^+]_i$ and pH_i assumed to be 50 mM and 7.0, respectively; pH_o = 5.8; then E_{KH} = −82, −64, −54, and −35 mV, respectively, for the four K^+ test pulses

amino acid transport (Sanders, Slayman & Pall, 1983) in *Neurospora*, amino acid and amine transport in *Riccia* (Felle, 1980, 1981*b*), and Cl^- transport in *Chara* (Beilby & Walker, 1981). Difference currents for all these transport systems proved largely independent of V_m, suggesting that the transport reversal potentials must lie well positive to the physiological voltage range.

Figure 3*A*, however, shows that for the K^+-H^+ system in *Neurospora* the apparanet K^+-induced currents were strongly voltage dependent, with slope conductances of 10–30 μS/cm^2 (for 5–200 μM K^+, respectively) in the neighborhood of −200 mV. The curves emphasize that for this K^+-H^+ symport, membrane potential itself—quite apart from other kinetic or regulatory factors—can have a profound effect on transport operation. A more surprising result was the failure of *all* ΔI-V curves for the K^+-H^+ symport to intersect the voltage axis, despite our expectation that the range of accessible membrane potentials should include the reversal potential for symport (E_{KH}): −82 to −35 mV, for $[K^+]_o$ = 5 to 200 μM. Tests of a variety of hypotheses and possible transport stoichiometries (*see* Table III of Rodriguez-Navarro et al., 1986) led to a realization that the failure to find E_{KH} must be a spurious result of the difference *I-V* technique (Blatt, 1986). A detailed analysis of ΔI-V curves has been published elsewhere (Blatt, 1986). For present purposes it is sufficient to note that two important conditions must be met for the technique to be valid: (i) the experimental treatment (here, addition or removal of potassium) affects *specifically and only* the particular transport system being investigated, as has already been discussed in connection with the proton pump (Gradmann et al, 1978) and the sodium pump (Chapman et al., 1983); and (ii) in the absence of substrate (here, $[K^+]_o$ = 0), current through the particular transport system in question is *everywhere zero*.

For the K^+-starved spherical cells of *Neurospora*, with 5–200 μM K^+ added to the extracellular medium, the first condition is indeed reasonably met. As noted above, the major components of the control membrane *I-V* relationship are the proton pump and a nonlinear leak, manifest as the steeply rising *outward* current at strong depolarization. The proton pump of fungi does not transport potassium (Amory et al., 1982; Perlin et al., 1984); and enzyme recovered in everted membrane vesicles is only weakly stimulated by 10–100 mM K^+ (Bowman & Slayman, 1977), presumably by reaction with the physiological inner surface of the pump. Furthermore, the nonlinear leak, which may conduct potassium ions [*see* discussion of Eqs. (2) and (3), above], could contribute only a negligible *change* of membrane current. This conclusion emerges from limit calculations with Eqs. (3), assuming *all* of the

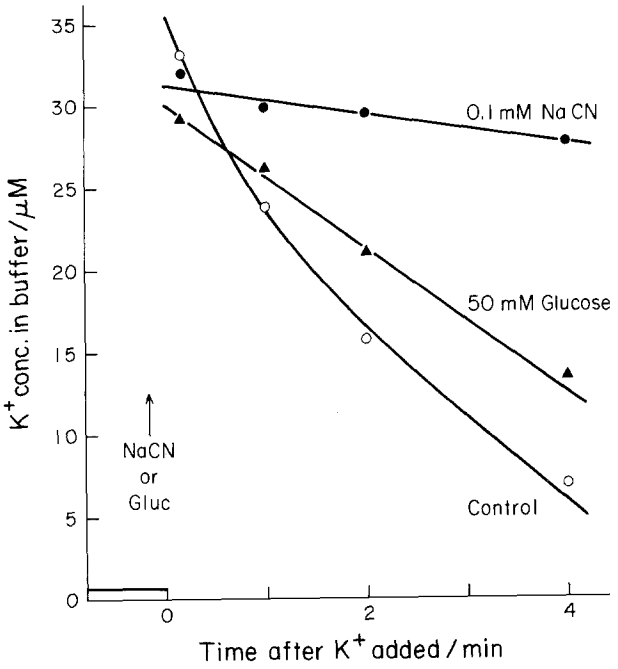

Fig. 4. Inhibitory effects of cyanide and glucose on potassium uptake via the K^+-H^+ symport in *Neurospora*. Cells were preincubated 10 min in the standard Ca-MES buffer at pH 5.8; 30 μM KCl was added at 0 time. In the test cases, 0.1 mM NaCN or 50 mM glucose was injected 10 sec ahead of K^+. At the indicated times (+10 sec, 1 min, 2 min, 4 min) the suspension was sampled and filtered. Potassium concentration in the filtrate was assayed by flame photometry. Cell density in the suspensions was determined on parallel samples, from which the cells were harvested, rinsed in distilled water, dried overnight, and weighed. Each plotted point is the average for two determinations, one with K^+-starved mycelium (*see* methods in Rodriguez et al., 1986) and one with low-K^+ spherical cells. The observed decline of $[K^+]_o$ can be translated into cellular uptake for the mycelium, using the factor intracellular water/dry weight = 2.54 (Slayman & Tatum, 1964), to give 4.1, 1.2, and 0.25 mM/min, for initial rates of K^+ uptake in the control, glucose, and NaCN cases, respectively

leakage current to be carried by potassium. For the curves of Fig. 2, an upper-limit estimate of leakage current at, e.g., V_m = (+)100 mV is 10 μA/cm^2; "zero" $[K^+]_o$ is about 0.5 μM, and $[K^+]_i$ is 50 mM (composition of the pipette-filling solution). With these numbers, Eq. (3) gives an apparent permeability for K^+ ($P_X = P_{K^+}$) of 5×10^{-7} cm/sec. Putting this back into Eq. (3), with different membrane potentials and 50 μM K^+ added to the medium, gives ~0 current shift at 100 mV, −0.01 μA/cm^2 at −100 mV, and −0.03 μA/cm^2 at −300 mV. Finally, it must be added that the depolarization and repolarization which accompany rapid addition and removal of K^+ (Fig. 2, inset) occur within range of the membrane's *RC* time constant (20–50 msec) and therefore give no indication of secondary, indirect effects by which added K^+ might alter pump or leak currents.

Unfortunately, however, the second condition required for the simple ΔI-V calculation to be valid is clearly not met for the K^+-H^+ symport. Because the cytoplasmic concentrations of both the substrate ion ($[K^+]_i \simeq 50$ mM) and the co-ion ($[H^+]_i \simeq 0.1$ μM) are appreciable at all times in these experiments, strong depolarization or reversed membrane potentials should produce an *outward current* through the symport *even when extracellular K^+ is zero*. Thus in the region positive to −100 mV, the control I-V curves of Figs. 1*B* and 2, as well as the test curves, should contain a component of symport current. Under such circumstances, simple I-V subtraction must give negative currents and negative slopes with strong depolarization (Blatt, 1986). Fortunately for practical purposes in the present experiments, ΔI-V results at membrane potentials negative to about −125 mV contain negligible subtraction error, and detailed fits over a wider range can be obtained by explicit use of the difference I-V equations (*see* Appendix, and Blatt, 1986).

It is possible to extract a more realistic, though still qualitative, view of symport kinetics from diagrams like that in Fig. 3*A*, by extrapolating the curves from large negative voltages through the cotransport reversal potentials (E_{KH}) calculated from single-ion diffusion potentials (E_K, E_H):

$$E_{KH} = 0.5(E_K + E_H) \quad (4)$$

which was derived explicitly in Rodriguez et al. (1986). This maneuver has been carried out in Fig. 3*B*, with the additional constraint that the saturating current at positive membrane potentials should be independent of the *extracellular* concentration of potassium ions. It can be seen that, at least within the range of experimentally accessible membrane potentials, the K^+-H^+ symport functions asymmetrically, allowing current to pass more easily in the inward direction (negative) than in the outward direction (positive), for a given voltage displacement from E_{KH}. An interpretation of this finding, in terms of relative sizes of reaction constants in cyclic reaction schemes for the symport, will be given later.

Action of Inhibitors on Potassium Transport

Although it would be useful for future experiments, we have not yet identified an inhibitor which is specific for the K^+-H^+ symport. High-affinity K^+ uptake is, however, quickly blocked by general metabolic inhibitors such as cyanide (Rodriguez-Navarro et al., 1986), and—more interestingly—is strongly inhibited by *transport* of other nutrients, such as glucose, which are not expected either to

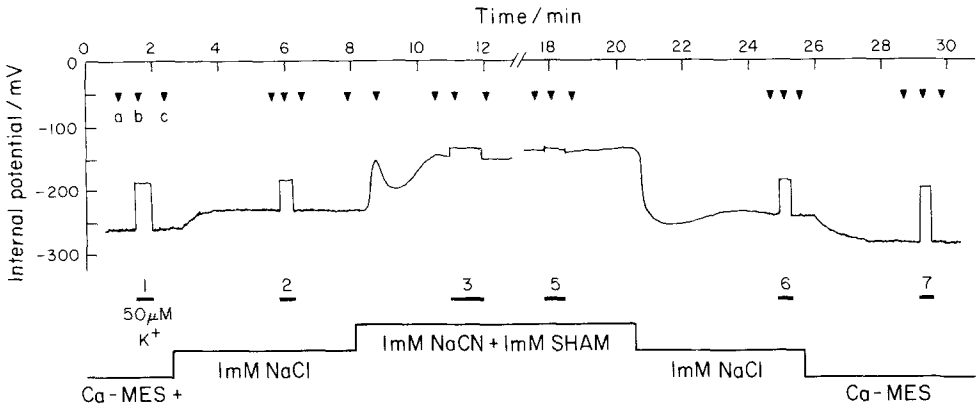

Fig. 5. Effect of respiratory inhibition upon K^+-evoked depolarization via the K^+-H^+ symport. Repeated testing of K^+ pulses (50 μM) in buffer, in buffer + 1 mM NaCl (salt control), and in buffer + cyanide and salicylhydroxamic acid (SHAM). SHAM was used to block a cyanide-insensitive terminal oxidase present in *Neurospora* under certain conditions (Lambowitz et al., 1972). Sensitivity of the cotransport system to membrane potential is indicated by the fact that prior depolarization of ca. 40 mV (i.e., with NaCl) reduced the K^+ response by a similar amount, and prior depolarization of ca. 130 mV essentially abolished the K^+ response. *I-V* scans made at the carats, but for clarity, voltage deflections were masked from the record

deplete energy reserves or to react with the potassium transport system, per se. A simple demonstration of potassium uptake by K^+-depleted cells given 0.1 mM NaCN or 50 mM glucose is shown in Fig. 4. In that experiment, K^+-starved spherical cells were harvested, rinsed, and resuspended in air-bubbled K^+-free Ca-MES buffer. After equilibration (5 to 10 min), test flasks were injected with glucose or NaCN, and 10 sec later, ~30 μM KCl was added. At appropriate intervals, aliquots of the medium were removed, filtered, and analyzed for residual K^+. The initial rate of potassium removal from the medium (uptake by the cells) was diminished 70% by the presence of glucose, and 94% by cyanide.

In view of the fact that both cyanide and glucose caused depolarization (Slayman, 1965*b*; Slayman & Slayman, 1974) and the fact that current through the cotransport system was strongly voltage-dependent (Fig. 3), it seemed likely that membrane depolarization would be the common mechanism for inhibition of potassium uptake. To explore this general question more systematically, we carried out several current-voltage experiments of the type shown in Fig. 5. A K^+-depleted cell was impaled with the usual 2-barrelled microelectrode, and at intervals of approximately 5 min 50 μM K^+ was injected into the medium in 20- to 40-sec pulses. *I-V* scans were run just before, during, and just after each K-pulse (*see* carats). After the control response to potassium had been established, 1 mM NaCN was added to the chamber, and the K^+ and *I-V* testing were continued. Later (20.5 min) the cyanide was removed, and more control data were collected. In the experiment of Fig. 5, NaCl was introduced separately as a control for possible depolarization caused by Na^+ (Slayman, 1965*a*), and 1 mM SHAM (salicylhydroxamic acid) was added with the cyanide in order to block possible functioning of a CN-insensitive respiratory system in *Neurospora* (Lambowitz et al., 1972).

In this and all similar experiments, the depolarizing step produced by 50 μM K^+ was reduced by prior membrane depolarization, whether due to ionic effects on the membrane (Na^+) or to metabolic inhibition. Voltage-clamp analysis showed, however, that the *initial* effect of NaCN on current through the cotransport system was small when the clamp was used to counter the depolarizing effect of cyanide. This point is documented in Fig. 6*A*, which shows membrane *I-V* curves with and without potassium, in the presence and absence of cyanide. K^+ uptake from 50 μM solutions would occur at 184 mV, under control conditions (first K^+-pulse, Fig. 5) without the clamp, and that is a convenient voltage at which to compare the currents ± cyanide. The vertical arrow #1 measures the current, 1.95 $\mu A/cm^2$, flowing from other membrane transport systems (*viz.*, the proton pump) to drive K^+ entry during the control pulse. The vertical arrow #3 measures the corresponding voltage-compensated current after 2–3 min in cyanide, 1.55 $\mu A/cm^2$, for a reduction of 20%. Those numbers should be compared with the apparent K^+ current flowing *without voltage compensation* in the presence of cyanide (dashed arrow in Fig. 6*A*): 0.6 $\mu A/cm^2$, for a 70% reduction. Thus, the major effect of metabolic inhibitors upon K^+ transport is indeed mediated by membrane depolarization.

A more detailed picture of the cyanide effect is provded by data at longer times in cyanide and by comparison of the full ΔI-*V* curves, as shown in Fig. 6*B*. Considering only voltages negative to −125 mV

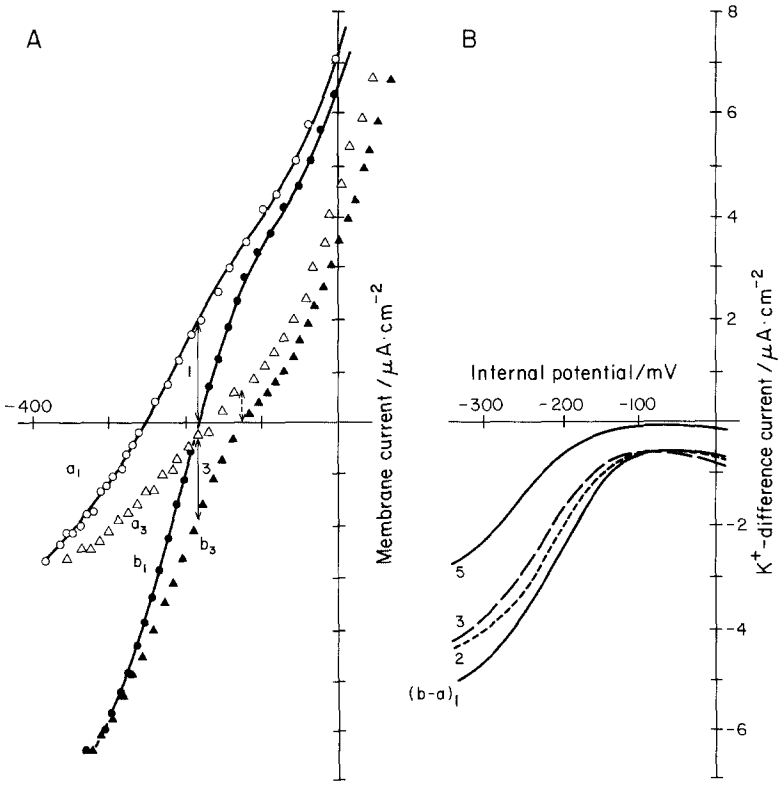

Fig. 6. Current-voltage analysis of K^+-H^+ cotransport during respiratory inhibition. (*A*) Control *I-V* data (○ and △) and K^+-pulse *I-V* data (● and ▲) for the first and third K^+ pulses in Fig. 5. Vertical arrows marked *1* and *3* designate the cotransport current stimulated by 50 μM K^+, *with membrane potential clamped at one reference point, viz.*, the potential assumed by the uninhibited cell in the presence of K^+. The unmarked vertical arrow designates the cotransport current in the cyanide-inhibited cell *without voltage clamping*. Smooth curves drawn through the control plots should be regarded for present purposes as "eye" fits. (*B*) Difference *I-V* curves for four K^+ pulses shown in Fig. 5, obtained by subtracting curve *a* from curve *b* for each pulse. Note that for at least 3 min cyanide had little effect beyond that produced by added salt, and that even after ca. 10 min its effect was limited to about 50% reduction of current, with little change in the kinetics (shape) of the Δ*I-V* relationship

(*see* above discussion of the Δ*I-V* technique), there are three salient features of this familiy of Δ*I-V* curves. First, much of the putative initial effect of NaCN was in fact obtained with NaCl (*compare* curve 3 with curve 2), and was probably related to Na^+, rather than to cyanide. Second, with prolonged treatment the cotransport system certainly was inhibited by cyanide, but slowly. Third, despite the considerable change in shape of the membrane *I-V* curves in the presence of the inhibitor (*cf.* curves a_1 and a_3, Fig. 6*A*), the K^+-difference *I-V* curves changed mostly in *amplitude*, with little alteration of shape. The latter fact suggests that both cyanide and sodium reduce the amount of cotransport system available to potassium. For Na^+, that effect could result directly from chemical competition between the two ion species (Ramos & Rodriguez-Navarro, 1985); for cyanide, it could result from protein turnover or a messenger-mediated control process.

A series of similar experiments was run using the specific H^+-pump blocking agent, orthovanadate. As had been shown previously (Kuroda et al., 1980), passage of vanadate ions through intact *Neurospora* membrane is slow, even when optimized by prior enhancement of a high-affinity phosphate transport system. We therefore used a four-barrelled microelectrode in order to inject the orthovanadate directly to the cell interior, and the voltage trace from such an experiment is shown in Fig. 7. In this case zero-time has been taken as the moment of electrode penetration, which was followed by the usual period for sealing of the membrane around the microelectrode, until a steady potential of about −260 mV was achieved. Irregularity of the voltage trace during sealing suggested that vanadate ions might be leaking into the cytoplasm, and positive current (150–300 pA) was applied to the injection electrode in order to hold VO_4 in the pipette. Several *I-V* scans (*see* carats) and a 35-sec pulse of 200 μM K^+ were given to establish control behavior, and then an injecting current of −165 pA was applied through the VO_4-pipette. After 8–10 sec the membrane potential collapsed to about −70 mV and remained there. Subsequent pulses of 200 μM K^+ (bars 2–4), applied at the prevailing membrane potential, elicited no perceptible depolarization.

I-V analysis, however, revealed the K^+-transport system to be fully active during the first 2 min of vanadate injection, as demonstrated in Fig. 8*A*. Here again the upper curves (circles) display the membrane *I-V* relationship in the absence (○) and presence (●) of extracellular K^+, and the vertical arrow #1 measures the current associated with normal K^+ entry, at the prevailing membrane potential of −159 mV. The lower plots (△, ▲) display the corresponding data obtained after about 100 sec of

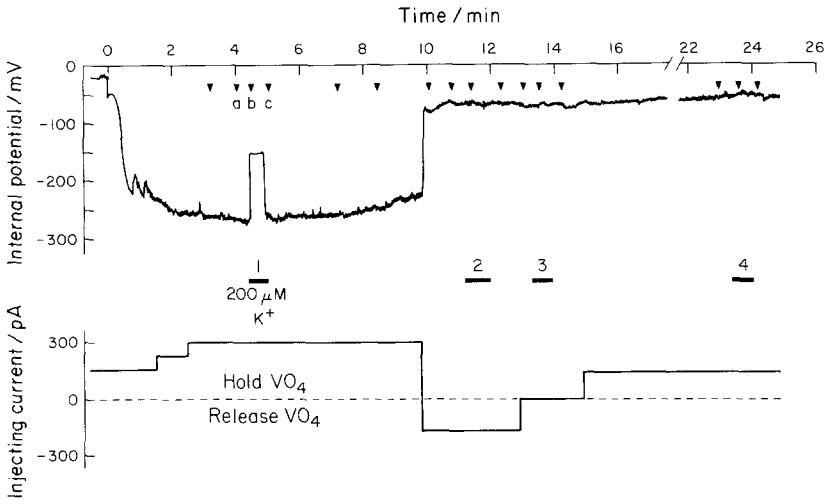

Fig. 7. Effect of H^+-pump blockade upon K^+-induced depolarization via the K^+-H^+ symport. Protocol was similar to that for Fig. 5, except that vanadate was injected into the cell from 5 mM solution in one barrel of the microelectrode (*see* Materials and Methods). Note that vanadate completely abolished the K^+-induced depolarization *in the absence of voltage clamping*. As in the experiment of Fig. 5, *I-V* scans were made at the carats, but for clarity, voltage deflections were masked from the record

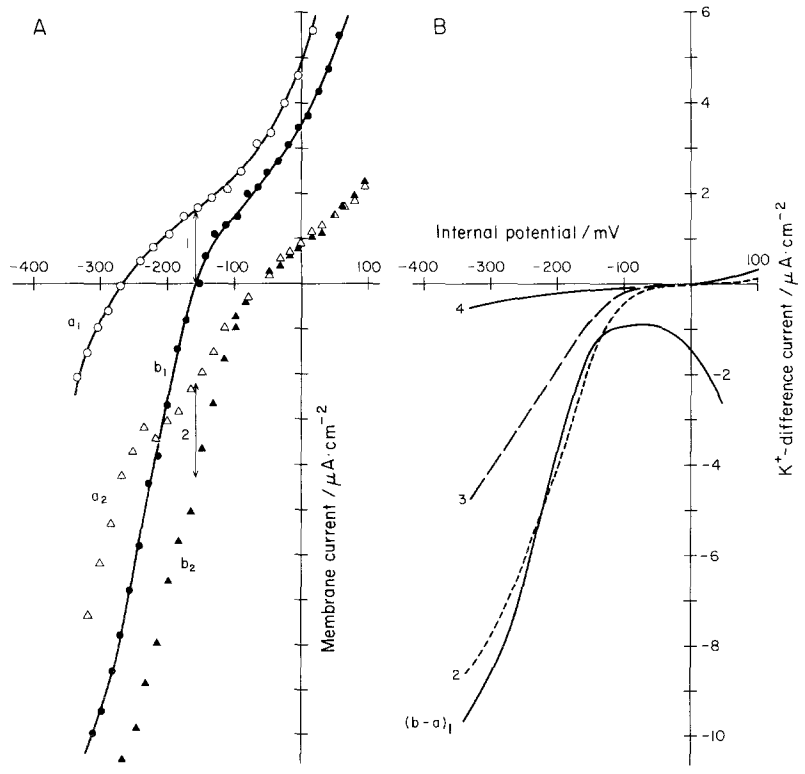

Fig. 8. Current-voltage analysis of K^+-H^+ cotransport during specific blockade of the H^+ pump. (*A*) Control *I-V* data (○ and △) and K^+-pulse *I-V* data (● and ▲) for the first and second K^+ pulses in Fig. 7. Vertical arrows marked *1* and *2* designate the cotransport current stimulated by 50 μM K^+, *with membrane potential clamped at one reference point, viz.*, the membrane potential assumed by the uninhibited cell in the presence of K^+. Again, curves drawn through the control plots should be regarded as "eye" fits. (*B*) Difference *I-V* curves for four K^+ pulses shown in Fig. 7, obtained by subtracting curve *a* from curve *b* for each pulse. Note that vanadate had no significant initial effect (at ca. 1 min), but it progressively reduced and linearized the K^+-induced current over 10–15 min

vanadate injection, and the vertical arrow #2 measures the K^+-associated current at the clamped potential of −159 mV. The latter current was 2.1 μA/cm², compared with 1.7 μA/cm² in the control case. Again we can conclude that the major route for vanadate inhibition of the K^+-H^+ symport is depolarization. The full Δ*I-V* curves (Fig. 8*B*) confirm this interpretation, but reveal a somewhat different course of events—compared with cyanide—during prolonged vanadate treatment. Vanadate eventually (curve 4) caused nearly complete deactivation of the K^+ transport system; and in progress it clearly changed the kinetic properties of the carrier, as reflected by linearization of the left branch of the Δ*I-V* curve (*compare* curves 3 and 4 with curves 1 and 2). The latter fact is difficult to interpret as far as the symport is concerned, but is a clear warning about nonspecificity in the overall action of vanadate ions (*see also* Tracey & Gresser, 1986; Swarup et al., 1982).

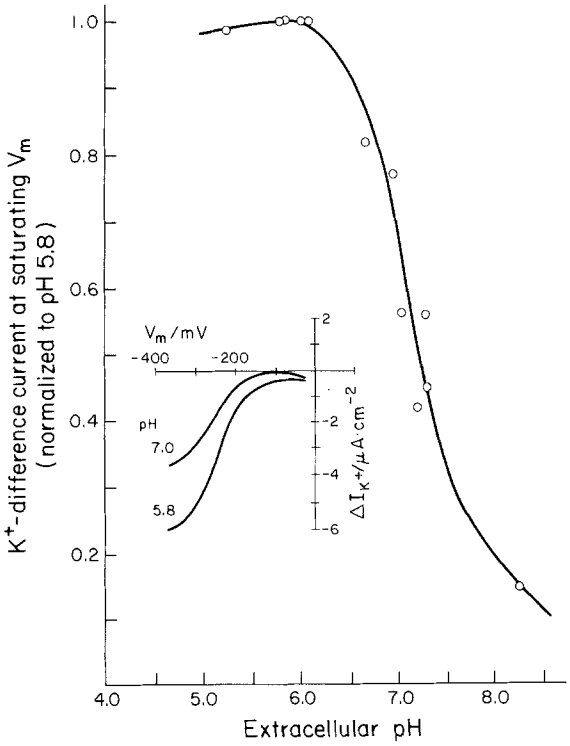

Fig. 9. Dependence of symport current on pH_o. Difference currents calculated for 50 μM-K^+ pulses, with membrane potential clamped at −320 mV. Aggregate data for three experiments, but with each value normalized to a companion measurement made on the same cell at pH 5.8. *Inset:* Sample K^+-difference curves from one cell, for pH 5.8 and pH 7.0

Kinetic Interaction of $[K^+]_o$, $[H^+]_o$, and V_m

Resting membrane potentials in K^+-starved spherical cells of *Neurospora*, absent metabolic and transport inhibitors, range between −300 and −100 mV. Thus, any measurements on the functioning K^+-H^+ transport system—whether K^+-difference currents, net K^+ fluxes, or isotopic (unidirectional) fluxes—are affected by at least five simple kinetic variables: V_m, $[K^+]_o$, $[K^+]_i$, $[H^+]_o$, and $[H^+]_i$. In most transport experiments (i.e., all experiments conducted without clamping of the membrane potential), only two of these variables, $[K^+]_o$ and $[H^+]_o$, are controlled. The two other concentration variables, $[K^+]_i$ and $[H^+]_i$, may be considered constant if short term (i.e., initial-rate) experiments are run. But V_m is utterly uncontrolled, so that the behavior of the transport system in response to changes of substrate or co-ion concentration cannot be understood or modeled without explicit knowledge of the concomitant voltage changes. Matters are complicated further by the fact that, over the same span of membrane potentials, current through the proton pump—and hence total current circulation through the membrane—is strongly voltage-dependent.

It is therefore not surprising that isotope-flux and net-K^+ uptake measurements on *Neurospora* show perceptibly non-Michaelian kinetics (Rodriguez-Navarro et al., 1986), nor that other fungi and plants which have similar-appearing potassium mechanisms can display very complicated kinetic variations. A major purpose of the present experiments, therefore, has been to create an explicit kinetic model of the *Neurospora* K^+-H^+ cotransporter, incorporating precise information on its relationship to membrane potential. In order to obtain a broad range of data for modeling, we carried out a series of experiments similar to that described in Figs. 2 and 3*A*, but varying both extracellular potassium levels and extracellular pH. In these experiments $[K^+]_i$ was held constant by the concentration-clamping effect of pipette-filling solutions (*see* Table III in Rodriguez-Navarro et al., 1986), and possible changes of pH_i were kept negligible by testing transport with only brief pulses of K^+ added.

The simplest result to describe is that the K^+-difference current (ΔI_{K^+}) at saturating membrane potentials (i.e., negative to ca. −320 mV) for any fixed $[K^+]_o$ declined steeply at pH values above 6, as is summarized in Fig. 9. The inset in Fig. 9 shows two sample ΔI-V curves obtained at different values of pH_o on a single cell tested with 50 μM K^+; quasi-saturating currents were read from the left end of each ΔI-V curve. Data for the main plot were assembled from three separate experiments, and cell-to-cell variation (about twofold for any particular condition; *cf.* Figs. 6*B* and 8*B* above) was minimized by dividing the value of ΔI_{K^+} obtained at each pH_o by the corresponding value at pH 5.8 in the same cell. It is clear that at pH_o values above 8 the high-affinity K^+ transporter became practically nonfunctional. That fact accounts for the old observation (H. Pfrüner and C.L. Slayman, *unpublished experiments*) that *Neurospora* can be depleted of potassium very rapidly at high pH.

A kinetically more meaningful view of the effect of extracellular pH on the cotransport system is given in Fig. 10. Part *A* shows a Lineweaver-Burk plot of the K^+-difference current at saturating voltage, for several different K^+ concentrations and three values of pH_o. It is readily apparent that extracellular protons behaved like a "competitive activator" of the transport system: decreasing pH_o (increasing $[H^+]_o$) caused the system K_m for extracellular potassium to decrease; that is, the apparent affinity of the transport system for its primary substrate ion increased along with the ambient concentration of its co-ion. The data could easily be described, however, with no change in maximal velocity ($\Delta I_{K^+(max)}$) of the transporter. A summary plot of the effects of extracellular pH on the maximal velocity and the Michaelis constant for K^+-H^+

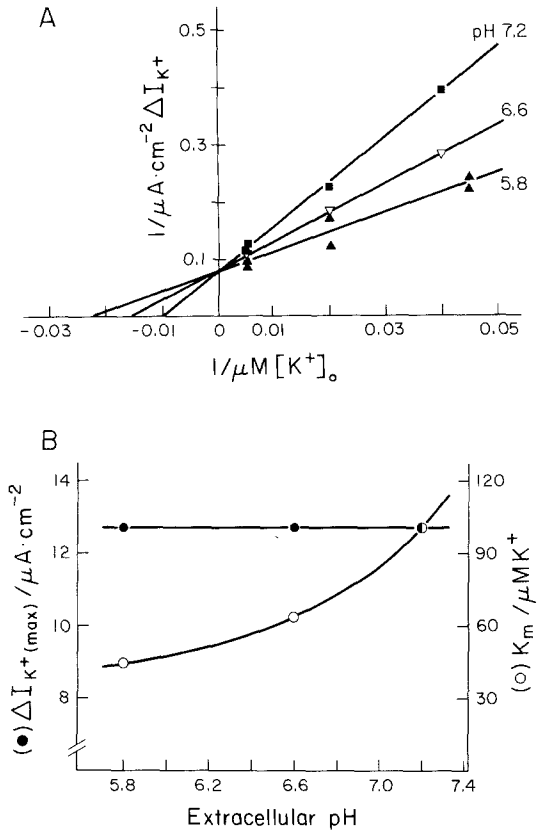

Fig. 10. pH-dependence of the kinetic parameters (I_{max}, K_m) for symport current, considered as a function of extracellular K^+ concentration. Methods as in Figs. 2 and 3, but data plotted only for saturating membrane potential (−320 mV). (*A*) Lineweaver-Burk plot of data. Straight lines positioned by eye, constrained to a common ordinate intercept. (*B*) Plot of kinetic parameters, as a function of extracellular pH, read from *A*. *Note:* H^+ concentration *falls* from left to right (pH_o rises), so that K_m *decreases* with *increasing* $[H^+]_o$. (●): I_{max}; (○): K_m. This kind of kinetic effect may be termed "competitive activation"

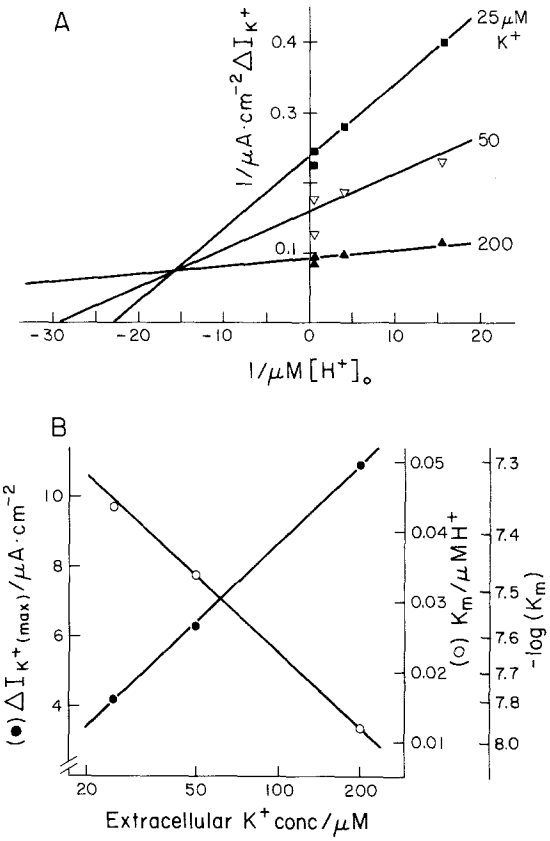

Fig. 11. K^+-dependence of the kinetic parameters (I_{max}, K_m) for symport current, considered as a function of extracellular H^+ concentration. Methods as in Figs. 2 and 3, but data plotted only for saturating membrane potential (−320 mV). (*A*) Lineweaver-Burk plot of data. Straight lines positioned by eye, constrained to a common intersection. (*B*) Plot of kinetic parameters, as a function of extracellular K^+, read from *A*. Symbols as in Fig. 10. Overall effect of K^+ on H^+ parameters represents "linear mixed-type activation"

cotransport is given in Fig. 10*B*. $\Delta I_{K^+(max)}$ was calculated in this experiment to be 12.7 μA/cm², and would imply a maximal K^+ influx of 6.35 μA/cm², or 66 pmol/cm² · sec.

[The above results differ from those previously reported on high-affinity rubidium transport in *Neurospora* (Rodriguez-Navarro & Ramos, 1986), for which the maximal velocity of transport rose along with $[H^+]_o$, at least over the pH range 8–5. We do not have a full explanation for the difference, which may have a significant methodological component, but there are at least two relevant biological factors. First, cells used in the rubidium experiments had been harvested from normal shaking cultures, and were K^+-starved without simultaneous carbon restriction or EG-treatment (*see* Materials and Methods); the two latter treatments have already been shown to modify the apparent kinetic properties of K^+ transport. Second, as was noted by Rodriguez-Navarro et al. (1986; Fig. 7), fluxes at very low $[K^+]_o$ tend to be unexpectedly large, but also scattered, so that precise kinetic analysis is difficult. The data plotted in Fig. 10, therefore, are restricted to test potassium concentrations of 20 μM and higher, and do not deal with the very low-concentration effects explored in the rubidium experiments. Whether the two ranges of data can be quantitatively accounted for by a common kinetic model will be addressed separately (C.L. Slayman & M.R. Blatt, *in preparation*).]

When the corresponding Lineweaver-Burk plot was made by treating H_o^+ (rather than K_o^+) as the substrate ion, a rather different picture emerged, as demonstrated in Fig. 11. By analogy with inhibitors affecting ordinary enzymes, extracellular K^+ behaved like a "linear mixed-type activator" (Segal, 1975), such that increasing $[K^+]_o$ caused the system K_m for protons to decrease, but caused the maximal

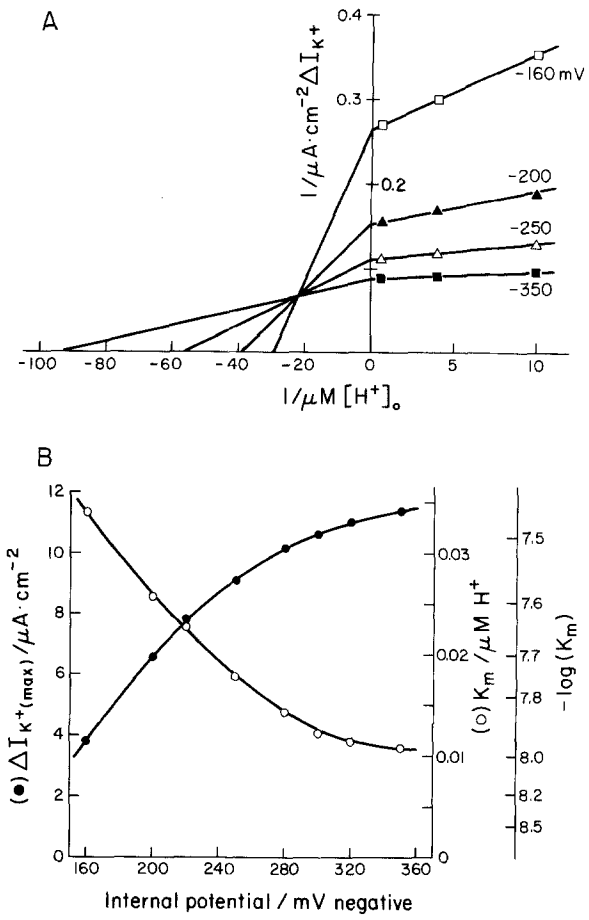

Fig. 12. Voltage-dependence of the kinetic parameters (I_{max}, K_m) for symport current, considered as a function of extracellular H^+ concentration. Methods as in Figs. 2 and 3, but data plotted for several membrane potentials with $[K^+]_o$ chosen to be saturating (200 μM). (*A*) Lineweaver-Burk plot of data. *Note:* abscissa scale compressed 10-fold on the left; right-hand plot was used to draw straight lines, constrained to a common intersection, and then left-half figure was redrawn for illustration. (*B*) plot of kinetic parameters, as a function of membrane potential, read from *A*. Symbols as in Fig. 10. Again, linear mixed-type activation

velocity of transport (at saturating voltage) to *increase* proportionately. Of particular physiological importance in this behavior is the fact that when $[K^+]_o$ = 20 μM, the apparent K_m for protons occurs at pH 7.3, while when $[K^+]_o$ = 200 μM, the system K_m occurs at pH 7.9 (*see* Fig. 11*B*). Both of these values are well above the normal acidic extracellular pH (5.8) for *Neurospora*, so the high-affinity K^+ transporter works well down to micromolar K^+ levels. However, raising extracellular pH (lowering $[H^+]_o$) lowers the carrier's apparent affinity for K^+ (Fig. 10); and lowering extracellular potassium lowers the carrier's apparent affinity for protons. The combination of these effects defeats high-affinity K^+ transport at high pH.

Sanders et al. (1984) found that the effect of membrane potential on transport kinetics discriminates more clearly among alternative reaction cycle models than does the effect of changing either the substrate or the co-ion. Double-reciprocal plots were therefore also used to analyze voltage effects superimposed upon changes of $[H^+]_o$ or $[K^+]_o$ as the primary variables. With respect to varied proton concentration, increasing (negative) membrane potential acted similarly to increasing $[K^+]_o$, as a "linear mixed-type activator"; the double-reciprocal plots are shown in Fig. 12*A*, for the case with $[K^+]_o$ fixed at 200 μM. Although they were not linearly related to membrane potential, $\Delta I_{K^+(max)}$ and $K_m(H^+)$ varied in inverse proportion to each other (Fig. 12*B*). Reducing V_m to (−)160 mV with K_o^+ = 200 μM was kinetically equivalent to reducing $[K^+]_o$ to 30 μM with V_m = (−)350 mV (*cf.* Figs. 11 and 12). Though approximate, this is an interesting statement of relative kinetic effectiveness for two variables which similarly affect proton binding to the K^+-H^+ symport: a sevenfold change of substrate ion concentration was equivalent to a 200-mV change of membrane potential. The thermodynamic equivalent of a 200-mV change would be a 2000-fold change of concentration!

With respect to varied potassium concentration, increasing membrane potential acted not like a simple "competitive activator," but instead like a "hyperbolic mixed-type activator" (again analogous to the nomenclature of Segal, 1975), such that both the maximal velocity of transport and the apparent K_m for K_o^+ increased simultaneously (Fig. 13). This surprising result suggested that K^+-binding should be remote from the charge transport step of the reaction cycle, and—together with the coherent effects of $[K^+]_o$ and V_m on the apparent proton affinity of the carrier—led to exploration of the ordered binding models presented in the Discussion.

Discussion

Selecting a Minimal Cyclic Reaction Scheme

Essentially all of the kinetic properties of the K^+-H^+ cotransport system can be described by means of one or two simple cyclic reaction models. In order to keep the models as simple and general as possible, we make no explicit physical assumptions other than to suppose that the transported ions tra-

verse the membrane by reacting cyclically with a species of protein molecule which is confined to the cell membrane. The models are conceived entirely in kinetic terms and in use are reduced to the smallest number of pseudo first-order reaction steps that the experimental data will permit. In keeping with the arguments of Hansen et al. (1981) and Sanders et al. (1984), no *a priori* assumption is made about which reaction steps are rate limiting. Voltage dependence is introduced, following the procedure of Läuger and Stark (1970), by assuming that charge-transit through the membrane occurs in a single reaction step, across a single symmetric Eyring barrier. Thus, the reaction constants for charge transit take the form

$$k_{io} = k_{io}^{o} \exp(zu/2) \quad \text{and} \quad k_{oi} = k_{oi}^{o} \exp(-zu/2) \quad (4)$$

where z is the number of charges crossing the membrane in the particular step; u (the "reduced membrane potential") is defined by $u \equiv FV_m/RT$; F, R, and T have their usual meanings; and k_{io}^{o} and k_{oi}^{o} denote rate constants for exit and entry, respectively, evaluated at zero membrane potential.

The simplest reaction cycle which is physically reasonable for a cotransport system is a six-state model in which the substrate ion and the co-ion bind (in either order) at one side of the membrane, then dissociate (in either order) at the other side. Three variants of this scheme capable of transporting two monovalent cations per cycle are diagrammed in the left column of Fig. 14. Model I (top) posits the "carrier" molecule itself to be electrically neutral so the charges actually transported are the bound cations; Model III (bottom) supposes that the dissociated carrier bears two negative charges, making the loaded carrier neutral; and Model II is the intermediate case.

Each diagram actually represents four possible reaction sequences, for the different orders of ion binding and release. However, because the major experiments reported above were carried out with $[K^+]_i$ clamped at 50 mM, and pH_i buffered near pH 7, little information was obtained about intracellular binding, and the 6-state models must therefore be reduced to pseudo 4- or 5-state models, shown in the right-hand column of Fig. 14. Our convention for naming reaction constants is also included on the reduced reaction diagrams; k's designate simple reaction constants, and K's designate lumped constants representing multiple steps. In fact, reaction constants for transitions adjacent to lumped sequences—e.g., k_{64} and k_{12} in Model I(R)—are also distorted by the lumping. A rigorous treatment of this effect could be given by dividing each designated constant by a "reserve factor" (viz., r_6 for k_{64} and r_1 for k_{12}) to accommodate unknown or inaccessible carried states. Properties of these reserve factors have been discussed elsewhere (Hanen et al., 1981; Sanders et al., 1984). However, for present purposes, we need not elaborate such complications. Reaction contants which contain either voltage or ion-concentration terms are expanded at the far right in Fig. 14 (k_{64} and k_{42} apply to all three models).

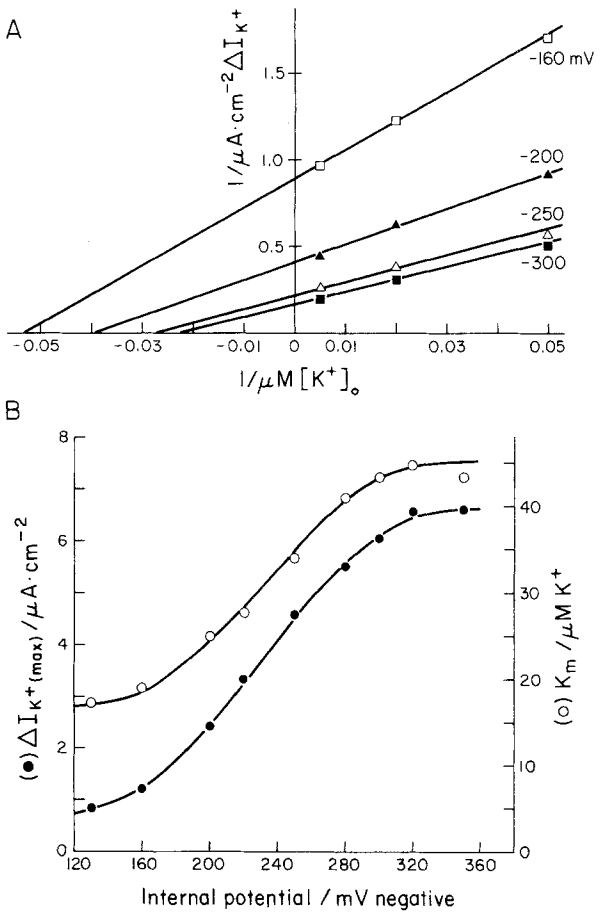

Fig. 13. Voltage-dependence of the kinetic parameters (I_{max}, K_m) for symport current, considered as a function of extracellular K^+ concentration. Methods as in Figs. 2 and 3, but data plotted for several membrane potentials with pH_o chosen to be saturating (pH 5.8). (*A*) Lineweaver-Burk plot of data. Straight lines positioned by eye, constrained to a common intersection (off scale). (*B*) Plot of kinetic parameters, as a function of membrane potential, read from *A*. Symbols as in Fig. 10. "Hyperbolic mixed-type activation"

Now, the data presented in Figs. 10–13 describe sets of saturation curves or "Michaelis curves" in which the maximal currents (J_{max}, = $I_{K^+(max)}$) and Michaelis constant (K_m), determined as functions of the substrate concentration ($[K^+]_o$ or

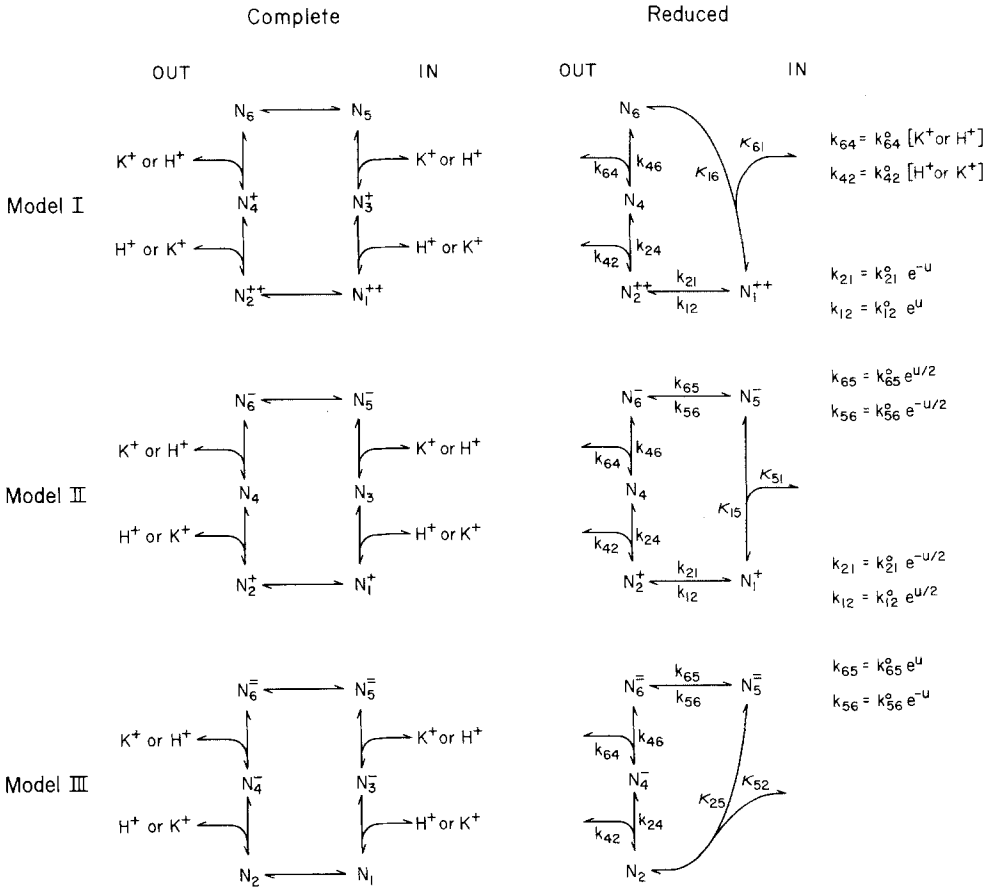

Fig. 14. Possible ordered-binding models for K^+-H^+ cotransport. Explicit 6-state schemes (left column) denote four possible binding and debinding orders for substrate (S^+) and driver ion (D^+). In the 4- and 5-state schemes on the right, binding steps inaccessible to direct manipulation (at the inside of the membrane) are lumped together, thus reducing the binding options in each case to two (S^+ first, D^+ last or vice versa). Reaction constants are indicated with ion-concentration and voltage terms written explicitly for each model; $u = FV_m/RT$. Nomenclature according to Sanders et al. (1984)

$[H^+]_o$) have been shown to vary systematically with the cosubstrate concentration ($[H^+]_o$ or $[K^+]_o$) and with membrane potential (V_m).

The general form of equation for current through any of the cotransport models in Fig. 14 is

$$I_{K^+} = 2F \frac{k_{12}|^1\mathbf{M}_m| - k_{21}|^2\mathbf{M}_m|}{|\mathbf{M}_m|} \qquad (5)$$

in which I_{K^+} is the current, m is the total number of states explicitly included in the model, $|\mathbf{M}_m|$ is the determinant for the characteristic matrix of coefficients for that model, $|^j\mathbf{M}_m|$ is the determinant for the adjusted matrix of coefficients excluding the jth state ($j = 1$ or 2), and the ratio $|^j\mathbf{M}_m|/|\mathbf{M}_m|$ gives the membrane content of the jth carrier state (i.e., N_1, or N_2). This equation holds for all three models in Fig. 14, despite the fact that in Model II half the total carrier current passes via the $N_5 \rightarrow N_6$ transition and in Model III all of the carrier current passes via that step, because the steady-state assumption means that net flow between N_5 and N_6 must equal the net flow between N_2 and N_1. [For practical purposes, it is usually simpler to write the numerator of Eq. (5) with the voltage-dependent reaction constants as coefficients: i.e., k_{12}, k_{21}, k_{65}, and k_{56} for Model II; and k_{65}, and k_{56} for Model III (*see* Appendix).]

All of the matrices in Eq. (5) and its congeners represent linear combinations of the model reaction constants, and although many terms in the numerator cancel, the net expression is non-Michaelian. There are, however, several experimentally attainable conditions which make the cotransport currents Michaelian in the extracellular substrate concentrations:

i) Membrane potential is clamped saturating and negative.

ii) One substrate ion concentration ($[K^+]_o$ or

TABLE 1. Summary list of conditions causing specified changes of K_m and J_{max} for substrate influx when membrane potential (V_m) or driver ion concentration ($[D^+]_o$) is varied.

Column Number:		1	2	3	4	Row #
Independent Variable:		V_m ($[D^+]_o$ saturating)		$[D^+]_o$ (V_m saturating)		
Model	Binding Order	K_m	J_{max}/(-)2FN	K_m	J_{max}/(-)2FN	
I(F)	S^+, D^+	$\frac{k^o_{12}e^{u}K_{61} + k^o_{21}e^{-u}(K_{16}+K_{61})}{k^o_{64}(k^o_{12}e^{u}+k^o_{21}e^{-u}+K_{16})}$	$\frac{k^o_{21}e^{-u}K_{16}}{k^o_{12}e^{u}+k^o_{21}e^{-u}+K_{16}}$	$\frac{(k^o_{42}[D^+]_o+k_{46})(K_{16}+K_{61})}{k^o_{64}(k^o_{42}[D^+]_o+K_{16})}$	$\frac{k^o_{42}[D^+]_oK_{16}}{k^o_{42}[D^+]_o+K_{16}}$	
	↑:	$K_{16} \gg k^o_{21}, k^o_{12}, K_{61}$	$K_{16} > k^o_{21}$ or $k^o_{12} \gg K_{16}, k^o_{21}$	$K_{16} \gg k^o_{42}[D^+]_o \gtrsim k_{46}$	$K_{16} \gg k^o_{42}[D^+]_o$	A
	↓:	NC; $K_m \sim 0$ if $K_{61} k^o_{21} \gg K_{16}$	NC; $J_{max} \sim 0$ if $k^o_{21} \gg K_{16}, k^o_{12}$	$k_{46} \gg k^o_{42}[D^+]_o \gtrsim K_{16}$	NC; $J_{max} \sim 0$ if $k^o_{42}[D^+]_o \gg K_{16}$	B
I(L)	D^+, S^+	$\frac{(k^o_{12}e^{u}+K_{16})k_{24} + k^o_{21}e^{-u}K_{16}}{k^o_{42}(k^o_{12}e^{u}+k^o_{21}e^{-u}+K_{16})}$	$\frac{k^o_{21}e^{-u}K_{16}}{k^o_{12}e^{u}+k^o_{21}e^{-u}+K_{16}}$	$\frac{(k^o_{64}[D^+]_o+k_{46})K_{16}+k_{46}K_{61}}{k^o_{42}(k^o_{64}[D^+]_o+K_{16}+K_{61})}$	$\frac{k^o_{64}[D^+]_oK_{16}}{k^o_{64}[D^+]_o+K_{16}+K_{61}}$	
	↑:	$K_{16} \gg k^o_{21}, k^o_{12}$	$K_{16} > k^o_{21}$ or $k^o_{12} \gg K_{16}, k^o_{21}$	$K_{16} \gg k^o_{64}[D^+]_o \gtrsim k_{46}, K_{61}$	K_{16} or $K_{61} \gg k^o_{64}[D^+]_o$	C
	↓:	$k_{24} \gg k^o_{21} \gtrsim k^o_{12}, K_{16}$	NC; $J_{max} \sim 0$ if $k^o_{21} \gg K_{16}, k^o_{12}$	$k_{46} \gg k^o_{64}[D^+]_o \gtrsim K_{61}, K_{16}$	NC; $J_{max} \sim 0$ if $k^o_{64}[D^+]_o \gg K_{16}, K_{61}$	D
II(F)	S^+, D^+	$\frac{k^o_{65}K_{51}(k^o_{12}e^{u}+k^o_{21}) + k^o_{21}K_{15}(k^o_{56}e^{-u}+k^o_{65})}{k^o_{64}\{k^o_{12}e^{u/2}(k^o_{56}e^{-u/2}+K_{51}) + k^o_{21}e^{-u/2}\cdot (K_{51}+K_{15}) + k^o_{56}e^{-u/2}(k^o_{21}e^{-u/2}+K_{15})\}}$	$\frac{k^o_{21}k^o_{56}e^{-u}K_{15}}{\{k^o_{12}e^{u/2}(k^o_{56}e^{-u/2}+K_{51}) + k^o_{21}e^{-u/2}\cdot (K_{51}+K_{15}) + k^o_{56}e^{-u/2}(k^o_{21}e^{-u/2}+K_{15})}$	$\frac{(k^o_{42}[D^+]_o+k_{46})K_{15}}{k^o_{64}(k^o_{42}[D^+]_o+K_{15})}$	$\frac{k^o_{42}[D^+]_oK_{15}}{k^o_{42}[D^+]_o+K_{15}}$	
	↑:	$K_{15} \gg k^o_{21}$	$K_{15} \gg k^o_{21}$	$K_{15} \gg k^o_{42}[D^+]_o \gtrsim k_{46}$	$K_{15} \gg k^o_{42}[D^+]_o$	E
	↓:	$k^o_{65} \gg k^o_{56}$, and $k^o_{21} \gtrsim K_{15}$	NC; $J_{max} \sim 0$ if $k^o_{21} \gg K_{15}$	$k_{46} \gg k^o_{42}[D^+]_o \gtrsim K_{15}$	NC; $J_{max} \sim 0$ if $k^o_{42}[D^+]_o \gg K_{15}$	F
II(L)	D^+, S^+	$\frac{k^o_{12}e^{u/2}k_{24}(k^o_{56}e^{-u/2}+K_{51}) + K_{15}k^o_{56}e^{-u/2}(k^o_{21}e^{-u/2}+k_{24})}{k^o_{42}[(k^o_{12}e^{u/2}+k^o_{21}e^{-u/2})(k^o_{56}e^{-u/2}+K_{51}) + K_{15}(k^o_{21}e^{-u/2}+k^o_{56}e^{-u/2})]}$	$\frac{k^o_{21}e^{-u/2}K_{15}[k^o_{12}e^{u/2}k_{24}(k^o_{56}e^{-u/2}+K_{51}) + K_{15}k^o_{56}e^{-u/2}(k^o_{21}e^{-u/2}+k_{24})]}{[(k^o_{12}e^{u/2}+k^o_{21}e^{-u/2})(k^o_{56}e^{-u/2}+K_{51}) + K_{15}\cdot (k^o_{21}e^{-u/2}+k^o_{56}e^{-u/2})][(k^o_{21}e^{-u/2}+k_{24})K_{15}+k^o_{12}e^{u/2}k_{24}]}$	$\frac{(k^o_{64}[D^+]_o+k_{46})K_{15}}{k^o_{42}(k^o_{64}[D^+]_o+K_{15})}$	$\frac{k^o_{64}[D^+]_oK_{15}}{k^o_{64}[D^+]_o+K_{15}}$	
	↑:	$K_{51} \gg k^o_{56}$, and $k^o_{21} \gtrsim k_{24}$	$k^o_{12} \gg k^o_{21}$, and $K_{51} \gg k^o_{56}$, and $k_{24} \gg k^o_{21}$	$K_{15} \gg k^o_{64}[D^+]_o \gtrsim k_{46}$	$K_{15} \gg k^o_{64}[D^+]_o$	G
	↓:	$k_{24} \gg k^o_{21} \gtrsim k^o_{12}$	NC	$k_{46} \gg k^o_{64}[D^+]_o \gtrsim K_{15}$	NC; $J_{max} \sim 0$ if $k^o_{64}[D^+]_o \gg K_{15}$	H
III(F)	S^+, D^+	$\frac{k^o_{65}e^{u}(K_{25}+K_{52}) + k^o_{56}e^{-u}K_{25}}{k^o_{64}(k^o_{56}e^{-u}+K_{25}+K_{52})}$	$\frac{k^o_{56}e^{-u}K_{25}}{k^o_{56}e^{-u}+K_{25}+K_{52}}$	$\frac{(k^o_{42}[D^+]_o+k_{46})K_{25}+k_{24}k_{46}}{k^o_{64}(k^o_{42}[D^+]_o+k_{24}+K_{25})}$	$\frac{k^o_{42}[D^+]_oK_{25}}{k^o_{42}[D^+]_o+k_{24}+K_{25}}$	
	↑:	K_{25} or $K_{52} \gg k^o_{56} \gtrsim k_{63}$	K_{25} or $K_{52} \gg k^o_{56}$	$K_{25} \gg k^o_{42}[D^+]_o, k_{46}, k_{24}$	K_{25} or $k_{24} \gg k^o_{42}[D^+]_o$	I
	↓:	$K_{52} \gg K_{25}, k^o_{56}$ or $k^o_{65} \gg k^o_{56}$	NC; $J_{max} \sim 0$ if $k^o_{56} \gg K_{25}, K_{52}$	$k_{46} \gg k^o_{42}[D^+]_o \gtrsim k_{24}, K_{25}$	NC; $J_{max} \sim 0$ if $k^o_{42}[D^+]_o \gg K_{25}, k_{24}$	J
III(L)	D^+, S^+	$\frac{k^o_{56}e^{-u}(k_{24}+K_{25}) + k_{24}K_{52}}{k^o_{42}(k^o_{56}e^{-u}+K_{25}+K_{52})}$	$\frac{k^o_{56}e^{-u}K_{25}}{k^o_{56}e^{-u}+K_{25}+K_{52}}$	$\frac{(k^o_{64}[D^+]_o+k_{46})(k_{24}+K_{25})}{k^o_{42}(k^o_{64}[D^+]_o+K_{25})}$	$\frac{k^o_{64}[D^+]_oK_{25}}{k^o_{64}[D^+]_o+K_{25}}$	
	↑:	$K_{25} \gg k^o_{56} \gtrsim K_{52}$	K_{25} or $K_{52} \gg k^o_{56}$	$K_{25} \gg k^o_{64}[D^+]_o \gtrsim k_{46}$	$K_{25} \gg k^o_{64}[D^+]_o$	K
	↓:	NC; $K_m \sim 0$ if $k^o_{56} \gg K_{25}, K_{52}$	NC; $J_{max} \sim 0$ if $k^o_{56} \gg K_{25}, K_{52}$	$k_{46} \gg k^o_{64}[D^+]_o \gtrsim K_{25}$	NC; $J_{max} \sim 0$ if $k^o_{64}[D^+]_o \gg K_{25}$	L

$[H^+]_o$) is saturating. This also requires that the membrane potential be sufficiently negative to make the measured difference current closely approximate the true cotransport current (*see* Figs. 3 and 4).

iii) As shown previously by Blatt (1986), the actual difference current (ΔI_{K^+}), rather than the simple cotransport current, is calculated. Although the primary expressions for ΔI_{K^+} are algebraically complicated, setting $[K^+]_o = 0$ for the control measurement, and assuming finite values of $[K^+]_i$ and $[H^+]_i$ to be identical for test and control measurements, does yield ΔI_{K^+} in Michaelian form in $[K^+]_o$.

Outlines of the derivations for these three cases are given in the Appendix and limiting expressions for I_{max} and K_m are summarized in Table 1 ($J_{max} \equiv I_{max}$). Because $[K^+]_i$ and $[H^+]_i$ were not manipulated and were assumed stable, all expressions in Table 1 were obtained from the reduced cotransport model shown in the right-hand column of Fig. 14.

Identifying Competent Models

The problem of determining which of the models in Fig. 14 are actually feasible reduces to that of find-

ing a single set of conditions—that is, a size-ordering of reaction constants—in Table 1 which are internally consistent and satisfy the observations of Figs. 10–13. The search of Table 1 must be made keeping in mind that K^+ is treated as the primary substrate (S^+, Table 1) in Figs. 10 and 13, with H^+ as the cosubstrate or "driver" ion (D^+); and H^+ is treated as the primary substrate in Figs. 11 and 12, with K^+ as the driver ion. In all cases the net reaction is assumed to flow in the counterclockwise direction.

Detailed examination of Table 1 reveals that the data from Figs. 10 and 13, dealing with the effects of $[H^+]_o$ and V_m on J_{max} and K_m for potassium transport, can be described by any of the six models, except for a weak inconsisteny in Model II when K^+ binds last. [In columns 1 and 2, Line G of Table 1, the parallel increase of J_{max} and K_m with increasingly negative membrane potential (Fig. 13) appears to require k_{21}^o to be both larger and smaller than k_{24}. The requirements, however, are not absolute, but depend upon the ratios K_{51}/k_{56}^o and k_{12}^o/k_{21}^o.] Changes in K_m for potassium, therefore, are not able to discriminate among the six models.

The data of Figs. 11 and 12 on the other hand, seem to require inconsistencies for all of the models, and strong inconsistencies for two: Model I with K^+ binding last, and Model III with K^+ binding first. [With H^+ as the primary substrate and binding first in Model I, column 1-line B shows that there are no conditions for which the K_m for protons can fall as V_m becomes more negative (Fig. 12); and exactly the same conclusion holds with H^+ binding last in Model III, as shown in column 1-line L.] We can therefore rule out these two Models in further consideration of the kinetics of H^+-coupled K^+ uptake by *Neurospora*. A more positive statement of this result is that the kinetic interaction of membrane potential and proton concentration requires H^+ binding to occur adjacent to the voltage-dependent reaction step(s). The presence of two voltage-dependent steps in Model II thus relaxes the allowable reaction sequence.

The weak inconsistencies, with respect to data in Figs. 11 and 12, which occur in the remaining four models are of two kinds: first, in Model I (K^+ first-on) and Model III (K^+ last-on) problems arise only with the lumped reaction constants, K_{16} and K_{61} in Model I, and K_{25} in Model III. [This can be seen by comparing column 4-line C with column 3-line D (for Fig. 11), and column 2-line C with column 1-line D (for Fig. 12) in Model I; or by comparing column 4-line I with column 3-line J (for Fig. 11) in Model III.] The Models II (either binding order) have problems with one of the lumped constants (K_{15}), but also show the second kind of inconsistency: in the voltage-dependent reaction constants. Thus for Model II (K^+ first-on), Fig. 12 seems to require both $k_{21}^o \lesssim k_{12}^o$ [column 1-line H] and $k_{12}^o \gg k_{21}^o$ [column 2-line G]. A similar problem has already been noted for Model II (K^+ last-on), with respect k_{21}^o and k_{24} and Fig. 13.

Because there are more inconsistencies in the Models II than in either Model I (K^+ first-on) or Model III (K^+ last-on), and because they affect the parameters which are related directly to the experiments (k_{12}^o and k_{21}^o), rather than parameters related only indirectly to experiments (K_{15}, K_{61}, etc.), we have rejected the Models II for H^+-coupled K^+ transport on the grounds of likelihood. Obviously, this is not an absolute exclusion.

Thus, two plausible reaction schemes remain: Model I (K^+ first-on) and Model III (K^+ last-on). Actually, it is the latter which has the fewest problems in describing the data of Figs. 10–13 (only with respect to K_{25} and Fig. 11, as noted above), and which therefore seems most likely to be correct and to be applicable over the widest range of conditions. The required size-ordering of reaction constants for the two models can be summarized in two serial inequalities, as extracted from Table 1:

MODEL I (K^+ first-on):

$$k_{46} \gg k_{42}^o\,[H^+]_o \gg K_{16},\ k_{24} > k_{64}^o\,[K^+]_o > K_{61} > k_{21}^o > k_{12}^o \qquad (6b)$$

MODEL III (K^+ last-on):

$$k_{46} > k_{64}^o\,[H^+]_o > K_{25},\ k_{65}^o > k_{42}^o\,[K^+]_o > k_{24} > k_{56}^o > K_{52}. \qquad (6a)$$

These sequences are incorporated into the summary reaction diagrams of Fig. 15.

Salient Characteristics of the Two Models

Despite obvious differences, the two models share several prominent features, as listed below.

i) The voltage-dependent reaction steps in the forward direction (counterclockwise, k_{21}^o and k_{56}^o) are slow enough to be rate limiting at zero membrane potential, which gives the net transport reaction strong voltage dependence over the entire physiologic range of membrane potentials (Fig. 3*B*). The two models differ, however, in one aspect of voltage dependence, viz., the relative magnitudes of the forward reaction constants versus the backward ones (clockwise, k_{12}^o and k_{65}^o). In Model I, k_{21}^o/k_{12}^o is greater than unity, whereas in Model III, the ratio k_{56}^o/k_{65}^o is less than unity. This means that in Model I at zero voltage, binding of the two sub-

strates ($\rightarrow N_2$) would push the (+) charge entry; but in Model III (−) charge exit would not be pushed (by N_5), but pulled, again by formation of N_2. This arises as an essential consequence of the asymmetry in the direction of the reaction flow, versus the direction of charge flow.

ii) The lumped ligand-binding reactions (K_{61} or K_{52}) inside the cell are also among the slowest steps in the carrier cycle. The rate constant pairs $K_{16} \gg K_{61}$ and $K_{25} \gg K_{52}$ strongly favor the unbound carrier states N_6 and N_5. As a consequence, potassium-proton uptake is expected to be rather insensitive to changes of intracellular ligand concentrations. This prediction is consistent with the fact that potassium current is only weakly dependent on the potassium composition of the microelectrode-filling solution (Rodriguez-Navarro et al., 1986). It should be noted, however, that if the prevailing conditions for transport become such that net movement on the symport is outward, then both current and K^+ (ef)flux should be very sensitive to $[K^+]_i$ and/or pH_i, since the overall transport rate could be limited by scarcity of states N_1 (Model I) or N_2 (Model III).

iii) A third common feature, noted briefly several paragraphs above, relates to the order of binding. Both models require proton binding adjacent to the transmembrane charge transfer step, mainly to account for the decrease in K_m (increase in affinity) for protons as a function of increasing (−) membrane potential. Implicit in this behavior is the fact that the component driving forces of membrane potential and ΔpH are interactive. Similar results have been reported for H^+-glucose cotransport in *Chlorella* (Schwab & Komor, 1978), where they were ascribed to a "proton-conducting pore" or "proton well" (Komor & Tanner, 1980), like that proposed for transport-coupled ATP synthesis (*cf.* Mitchell, 1969; Maloney, 1982). For present experiments, however, this interaction can be accommodated entirely within the simple reaction-kinetic scheme, by placing $[H^+]$ binding and charge transfer in close proximity, with suitable ordering of the associated reaction constants (*see also* Sanders et al., 1984).

Further Implications

Although voltage sensitivity is in principle a feature of all rheogenic transport processes, the high-affinity K^+ transporter in *Neurospora* is unusual among described cotransport systems in that its region of steep voltage dependence lies within the normal range of physiologic membrane potentials. In most other cotransport systems studied to date (Hansen & Slayman, 1978; Felle, 1980, 1981*a*,*b*; Beilby & Walker, 1981; Sanders et al., 1984; Restrepo & Kimmich, 1985; Lapointe, Hudson & Schultz, 1986) the transport reversal potentials appear to be well positive to the normal membrane potentials (but *see* Blatt, 1986).

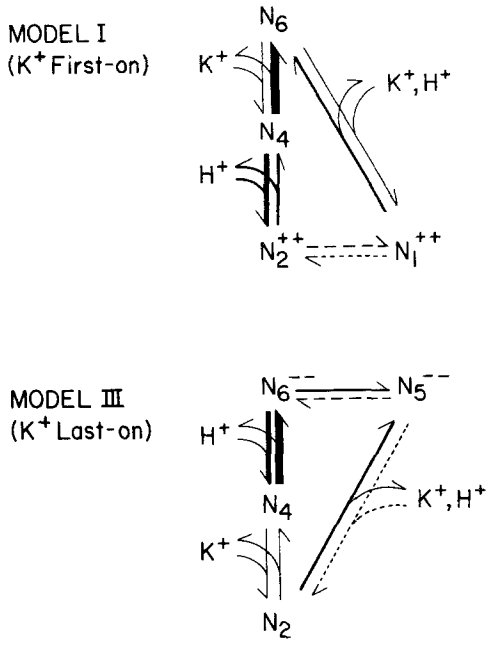

Fig. 15. Kinetically favored models for K^+-H^+ cotransport. These two schemes were extracted from Fig. 14 by comparison of Figs. 10–13 with kinetic parameters (I_{max}, K_m) in Table 1. Required relative reaction rates indicated by arrow thickness; net flow is counterclockwise

There are two important consequences of the arrangement for K^+ uptake in *Neurospora*. First, under ordinary conditions (without voltage clamping), potassium uptake can depart from the customary saturation behavior (Rodriguez-Navarro et al., 1986), with influx through the high-affinity system continuing to increase at $[K^+]_o$ values well above the K_m calculated from micromolar tests. Such behavior—dubbed a "dual isotherm" for transport—has been observed in a variety of plant-cell materials, and has been variously attributed to the presence of discrete but overlapping transport systems (Epstein, 1966; Nissen, 1973), to molecular "slip" within a single type of carrier (Eddy, 1980), to a critical static bias of reaction parameters in cotransport systems (Sanders, 1986), and to kinetic effects of diminishing membrane potential as the ion-substrate concentration is raised (Gerson & Poole, 1971). The latter mechanism is quite sufficient to account for the observations on EG cells of *Neurospora*, and indeed kinetic parameters derived from the *I-V* measurements of Figs. 10–13 closely predict the ion-flux data reported previously (Rodri-

guez-Navarro et al., 1986; Fig. 7), as will be demonstrated in a subsequent paper (C.L. Slayman and M.R. Blatt, *in preparation*).

The second consequence is that potassium uptake in *Neurospora* is very sensitive to activity of the (electrogenic) proton pump, and hence to the metabolic state of the cells. Uncritical interpretation of the inhibitory action of cyanide (Fig. 4), azide, and other metabolic inhibitors, upon K^+ influx would lead easily to the conclusion that potassium transport depends directly upon ATP hydrolysis. That such is not the case has clearly been shown by the fact that metabolic inhibitors and a specific pump inhibitor (orthovanadate) all rapidly block the K^+-associated current, but not if their depolarizing effects are prevented by means of a membrane voltage clamp (Figs. 6 and 8). It is thus possible to isolate potassium transport from direct effects on primary pumping or upon the ATP pool size. A similar conclusion might hold also for potassium transport sensitivity to DCCD in yeast (Peña, 1975; Hauer et al., 1981) and *Chlorella* (Tromballa, 1981) and to cyanide, vanadate, DCCD, DES and anoxia in higher plants (Poole, 1978; Cheeseman et al., 1980; Cocucci, Ballarin-Denti & Marrè, 1980; Mercier & Poole, 1980; Marrè, Romani & Marrè, 1983).

The slow direct blockade of K^+-H^+ transport by cyanide and vanadate remains unexplained, but their points of attack can be deduced from the models. CN inhibition leaves the basic kinetic properties of the transport system unaltered and therefore should affect only the total number of carriers (N_t) available for transport. Vanadate inhibition, on the other hand, does change the kinetics of transport, and in a manner which can be mimicked by retardation of the voltage-dependent transport steps. Whether either inhibitor reacts chemically with the K^+ system itself is unknown.

One final point bears mentioning in relation to the effects of intracellular pH on potassium transport activity. There are widespread reports that cytoplasmic acid-loading stimulates K^+ uptake: e.g., in yeast (Ryan, Ryan & O'Connor, 1971; Peña, 1975), *Chlorella* (Tromballa, 1978), and corn roots (Marrè et al., 1983). Furthermore, potassium starvation is known to reduce intracellular pH in yeast and *Chlorella;* and potassium uptake is accompanied by cytoplasmic alkalinization in a variety of organisms (Ryan et al., 1971; Peña, 1975; Tromballa, 1980; Marrè et al., 1983; Ogino et al., 1983). Such findings have led to the frequent proposal that intracellular pH *regulates* K^+ transport in plants and microorganisms. The evidence in Figs. 6 and 8 of this paper, together with the previously reported experiments on pH regulation, however, demonstrate a quite different interpretation of the pH effect on high-affinity K^+ uptake. That is stimulation of K^+ influx results from voltage-mediated kinetic control, arising secondarily to acid stimulation of the proton pump. This effect is analogous with—but opposite to—the rapid effects of cyanide and vanadate on K^+ influx. Whether the same interpretation can be given to results on yeast and plant cells awaits experimental testing.

The authors are indebted to Dr. Carolyn Slayman, Department of Human Genetics, Yale University, for use of laboratory facilities and for many helpful discussions. The work was supported by research grant GM-15858 from the National Institute of General Medical Sciences and by research grant DEFG02-85ER13359 from the United States Department of Energy. M.R.B. was a National Research Service Awardee (AM-07259), and A.R.-N. was a fellow of the Fundación Juan March, Spain.

References

Amory, A., Goffeau, A., McIntosh, D.B., Boyer, P.D. 1982. Exchange of oxygen between phosphate and water catalyzed by the plasma membrane ATPase from the yeast *Schizosaccharomyces pombe*. *J. Biol. Chem.* **257:**12509–12516

Barr, C.E., Holland, D.J., Bower, B.L. 1977. Promotion of H^+ extrusion in *Nitella* by external K^+. *In:* Transmembrane Ionic Exchange in Plants. M. Thellier, A. Monnier, M. DeMarty, and J. Dainty, editors. pp. 179–184. C.N.R.S., Paris

Beilby, M., Walker, N.A. 1981. Chloride transport in *Chara:* I. Kinetics and current-voltage curves for a probable proton symport. *J. Exp. Bot.* **32:**43–54

Blatt, M.R. 1986. Interpretation of steady-state current-voltage curves: Consequences and implications of current subtraction in transport studies. *J. Membrane Biol.* **92:**91–110

Blatt, M.R. 1987. Electrical characteristics of stomatal guard cells: The ionic basis of the membrane potential and the consequences of potassium chloride leakage from microelectrodes. *Planta (in press)*

Blatt, M.R., Slayman, C.L. 1983. KCl leakage from microelectrodes and its impact on the membrane parameters of a non-excitable cell. *J. Membrane Biol.* **72:**223–234

Blatt, M.R., Slayman, C.L. 1987. Role of "active" potassium transport in regulation of cytoplasmic pH by non-animal cells. *Proc. Natl. Acad. Sci. USA* **84:**2737–2741

Bowman, B., Slayman, C.W. 1977. Characterization of the plasma membrane adenosine triphosphatase of *Neurospora crassa*. *J. Biol. Chem.* **252:**3357–3363

Bowman, B., Slayman, C.W. 1979. The effects of vanadate on the plasma membrane ATPase of *Neurospora crassa*. *J. Biol. Chem.* **254:**2928–2934

Chapman, J.B., Johnson, E.A., Kootsey, J.M. 1983. Electrical and biochemical properties of an enzyme model of the sodium pump. *J. Membrane Biol.* **74:**139–153

Cheeseman, J., LaFayette, P., Gronewald, J., Hanson, J. 1980. Effect of ATPase inhibitors on cell potential and K^+ influx in corn roots. *Plant Physiol.* **65:**1139–1145

Cocucci, M., Ballarin-Denti, A., Marrè, M. 1980. Effects of orthovanadate on H^+ and K^+ transport, transmembrane potential and plasmalemma ATPase activity in plant tissues. *In:* Plant Membrane Transport: Current Conceptual Issues.

R.M. Spanswick, W.J. Lucas, and J. Dainty, editors. pp. 505–506. Elsevier, Amsterdam

Eddy, A.A. 1980. Slip and leak models of gradient-coupled solute transport. *Biochem. Soc. Trans.* **8:**271–273

Epstein, E. 1966. Dual pattern of ion absorption by plant cells and plants. *Nature (London)* **212:**1324–1327

Felle, H. 1980. Amine transport at the plasmalemma of *Riccia fluitans*. *Biochim. Biophys. Acta* **602:**181–195

Felle, H. 1981*a*. A study of the current-voltage relationships of the electrogenic active and passive membrane elements in *Riccia fluitans*. *Biochim. Biophys. Acta* **646:**151–160

Felle, H. 1981*b*. Stereospecificity and electrogenicity of amino acid transport in *Riccia fluitans*. *Planta* **152:**505–512

Gerson, D.F., Poole, R.J. 1971. Anion absorption by plants: A unitary interpretation of "dual mechanisms." *Plant Physiol.* **48:**509–511

Gradmann, D. 1975. Analog circuit of the *Acetabularia* membrane. *J. Membrane Biol.* **25:**183–208

Gradmann, D., Hansen, U.-P., Long, W.S., Slayman, C.L., Warnke, J. 1978. Current-voltage relationships for the plasma membrane and its principal electrogenic pump in *Neurospora crassa*. I: Steady-state conditions. *J. Membrane Biol.* **59:**333–367

Gradmann, D., Hansen, U.-P., Slayman, C.L. 1982. Reaction-kinetic analysis of current-voltage relationships for electrogenic pumps in *Neurospora* and *Acetabularia*. *Curr. Top. Membr. Trans.* **16:**257–276

Hansen, U.-P., Gradmann, D., Sanders, D., Slayman, C.L. 1981. Interpretation of current-voltage relationships for "active" ion transport systems: I. Steady-state reaction-kinetic analysis of class I mechanisms. *J. Membrane Biol.* **63:**165–190

Hansen, U.-P., Slayman, C.L. 1978. Current-voltage relationships for a clearly electrogenic cotransport system. *In:* Membrane Transport Processes. J.F. Hoffman, editor. pp. 141–154. Raven, New York

Hauer, R., Uhlemann, G., Neumann, J., Höfer, M. 1981. Proton pumps of the plasmalemma of the yeast *Rhodotorula gracilis:* Their coupling to fluxes of potassium and other ions. *Biochim. Biophys. Acta* **649:**680–690

Hodgkin, A.L., Katz, B. 1949. The effect of sodium ions on the electrical activity of the giant axon of the squid. *J. Physiol. (London)* **108:**37–77

Komor, E., Tanner, W. 1980. Proton-cotransport of sugars in plants. *In:* Plant Membrane Transport: Current Conceptual Issues. R.M. Spanswick, W.J. Lucas, and J. Dainty, editors. pp. 247–257. Elsevier, Amsterdam

Kuroda, H., Warncke, J., Sanders, D., Hansen, U.-P., Allen, K.E., Bowman, B.J. 1980. Effects of vanadate on the electrogenic pump in *Neurospora*. *In:* Plant Membrane Transport: Current Conceptual Issues. R.M. Spanswick, W.J. Lucas, and J. Dainty, editros. pp. 507–508. Elsevier, Amsterdam

Lambowitz, A.M., Slayman, C.W., Slayman, C.L., Bonner, W.D. 1972. The electron transport components of wild-type and *poky* strains of *Neurospora crassa*. *J. Biol. Chem.* **247:**1536–1545

Lapointe, J.-Y., Hudson, R.L., Schultz, S.G. 1986. Current-voltage relations of sodium-coupled sugar transport across the apical membrane of *Necturus* small intestine. *J. Membrane Biol.* **93:**205–220

Läuger, P., Stark, G. 1970. Kinetics of carrier-mediated ion transport across lipid bilayer membranes. *Biochim. Biophys. Acta* **211:**458–466

Leonard, R.T. 1982. Potassium transport and the plasma membrane-ATPase in plants. *In:* Metals and Micronutrients: Uptake and Utilization by Plants. D.A. Robb and W.S. Pierpoint, editors. pp. 71–86. Academic, London

Lin, W., Hanson, J.B. 1976. Cell potentials, cell resistance, and proton fluxes in corn root tissue. Effects of dithioerythritol. *Plant Physiol.* **58:**276–282

Maloney, P.C. 1982. Energy coupling to ATP synthesis by the proton-translocating ATPase. *J. Membrane Biol.* **67:**1–12

Marquardt, D. 1963. An algorithm for least-squares estimation of non-linear parameters. *J. Soc. Ind. Appl. Math.* **11:**431–441

Marrè, M., Romani, G., Marrè, E. 1983. Transmembrane hyperpolarization and increase of K^+ uptake in maize roots treated with permeant weak acids. *Plant Cell Environ.* **6:**617–623

Mercier, A.J., Poole, R.J. 1980. Electrogenic pump activity in red beet: Its relation to ATP levels and to cation influx. *J. Membrane Biol.* **55:**165–174

Mitchell, P. 1969. Chemiosmotic coupling and energy transduction. *Theoret. Exp. Biophys.* **2:**159–216

Nissen, P. 1973. Kinetics of ion uptake in higher plants. *Physiol. Plant.* **28:**113–120

Ogino, T., Hollander, J. den, Shulman, R. 1983. ^{39}K, ^{23}Na and ^{31}P-NMR studies of ion transport in *Saccharomyces cerevisiae*. *Proc. Natl. Acad. Sci. USA* **80:**5185–5190

Peña, A. 1975. Studies on the mechanism of K^+ transport in yeast. *Arch. Biochem. Biophys.* **167:**397–409

Perlin, D.S., Kasamo, K., Brooker, R.J., Slayman, C.W. 1984. Electrogenic H^+ translocation by the plasma membrane ATPase of *Neurospora*. *J. Biol. Chem.* **259:**7884–7892

Poole, R. 1978. Energy coupling for membrane transport. *Annu. Rev. Plant Physiol.* **29:**437–460

Ramos, J., Rodriguez-Navarro, A. 1985. Rubidium transport in *Neurospora crassa*. *Biochim. Biophys. Acta* **815:**97–101

Restrepo, D., Kimmich, G.A. 1985. The mechanistic nature of the membrane potential dependence of sodium-sugar cotransport in small intestine. *J. Membrane Biol.* **87:**159–172

Rodriguez-Navarro, A., Blatt, M.R., Slayman, C.L. 1986. A potassium-proton symport in *Neurospora crassa*. *J. Gen. Physiol.* **87:**649–674

Rodriguez-Navarro, A., Ramos, J. 1986. Two systems mediate rubidium uptake in *Neurospora crassa:* One exhibits the dual-uptake isotherm. *Biochim. Biophys. Acta* **857:**229–237

Ryan, H., Ryan, J., O'Connor, W. 1971. The effect of diffusible acids on potassium ion uptake by yeast. *Biochem. J.* **125:**1081–1085

Sanders, D. 1986. Generalized kinetic analysis of ion-driven cotransport systems: II. Random ligand binding as a simple explanation for non-Michaelian kinetics. *J. Membrane Biol.* **90:**67–87

Sanders, D., Hansen, U.-P., Gradmann, D., Slayman, C.L. 1984. Generalized kinetic analysis of ion-driven cotransport systems: A unified interpretation of selective ionic effects on Michaelis parameters. *J. Membrane Biol.* **77:**123–152

Sanders, D., Slayman, C.L. 1982. Control of intracellular pH: Predominant role of oxidative metabolism, not proton transport, in the eukaryotic microorganism *Neurospora*. *J. Gen. Physiol.* **80:**377–402

Sanders, D., Slayman, C.L., Pall, M. 1983. Stoichiometry of H^+/amino acid cotransport in *Neurospora crassa* revealed by current-voltage analysis. *Biochim. Biophys. Acta* **735:**67–76

Schwab, W., Komor, E. 1978. A possible mechanistic role of the membrane potential in proton-sugar cotransport of *Chlorella*. *FEBS Lett.* **87:**157–160

Segal, I.H. 1975. Enzyme Kinetics: Behavior and Analysis of

Rapid Equilibrium and Steady-State Enzyme Systems: Wiley-Interscience, New York.

Slayman, C.L. 1965*a*. Electrical properties of *Neurospora crassa:* Effects of external cations on the intracellular potential. *J. Gen. Physiol.* **49:**69–92

Slayman, C.L. 1965*b*. Electrical properties of *Neurospora crassa:* Respiration and the intracellular potential. *J. Gen. Physiol.* **49:**93–116

Slayman, C.L., Slayman, C.W. 1974. Depolarization of the plasma membrane of *Neurospora* during active transport of glucose: Evidence for a proton-dependent cotransport system. *Proc. Natl. Acad. Sci. USA* **71:**1935–1939

Slayman, C.W., Tatum, E.L. 1964. Potassium transport in *Neurospora:* I. Intracellular sodium and potassium concentrations, and cation requirements for growth. *Biochim. Biophys. Acta* **88:**578–592

Swarup, G., Speeg, K.V., Jr., Cohen, S., Garbers, D.L. 1982. Phosphotyrosylprotein phosphatase of TCRC-2 cells. *J. Biol. Chem.* **257:**7298–7301

Tracey, A.S., Gresser, M.J. 1986. Interaction of vanadate with phenol and tyrosine: Implications for the effects of vanadate on systems regulated by tyrosine phosphorylation. *Proc. Natl. Acad. Sci. USA* **83:**609–613

Tromballa, H.W. 1978. Influence of permeant acids and bases on net potassium uptake by Chlorella. *Planta* **138:**243–246

Tromballa, H.W. 1980. Electrogeneity of potassium transport in *Chlorella. Zeit. Pflanzenphysiol.* **96:**123–133

Tromballa, H.-W. 1981. The effect of the uncoupler carbonyl cyanide *m*-chlorophenylhydrazone on K^+ transport, ATP level, and intracellular pH of *Chlorella fusca. Biochim. Biophys. Acta* **636:**98–103

Vogel, H.J. 1956. A convenient growth medium for *Neurospora* (Medium N). *Microb. Genet. Bull.* **13:**42–46

Received 9 March 1987; revised 8 May 1987

Appendix

Outline of Derivations: Saturating Voltage or Substrate

Steady-state ion currents through single-loop carrier schemes like those diagrammed in Fig. 14 are given by text Eq. (5)

$$I_{K^+} = 2F\frac{k_{12}|^1\mathbf{M}_m| - k_{21}|^2\mathbf{M}_m|}{|\mathbf{M}_m|} \tag{5}$$

in which $|^1\mathbf{M}_m|/|\mathbf{M}_m|$ and $|^2\mathbf{M}_m|/|\mathbf{M}_m|$ are the determinant solutions for the apparent steady-state level of carrier in the two states N_1 and N_2. Because of symmetry in the determinants $|^1\mathbf{M}_m|$ and $|^2\mathbf{M}_m|$, all but two terms in the expanded numerator cancel; and each remaining term is the product of all reaction constants around the carrier cycle in one direction (i.e., clockwise for k_{12} and counterclockwise for k_{21}). Since $|\mathbf{M}_m|$, the determinant of the characteristic matrix for the reaction, represents a linear sum of simple products of the reaction constants, the denominator of Eq. (5) can always be written in the form $A + Bk^o[S^+]_o$, where all terms containing the operational primary substrate ($[K^+]_o$ *or* $[H^+]_o$ in these experiments) are segregated into B, and all terms not containing $[S^+]$ are lumped into A. A and B are in general functions of membrane potential (V_m) and the cosubstrate concentration, $[D^+]_o$ ($[H^+]_o$ *or* $[K^+]_o$).

In Model I, for example, the numerator of Eq. (5) is

$$N(k_{12}k_{24}k_{46}K_{61} - k_{21}k_{42}k_{64}K_{16}) \tag{A1}$$

and the denominator is

$$\begin{aligned}&k_{21}k_{42}(k_{64} + K_{61}) + K_{61}k_{46}(k_{24} + k_{21}) + k_{12}K_{61}(k_{46} + k_{42})\\ &+ k_{42}k_{64}(K_{16} + k_{12}) + K_{16}k_{21}(k_{42} + k_{46}) + k_{46}k_{24}(k_{12} + K_{16})\\ &+ k_{24}k_{12}(K_{61} + k_{64}) + k_{64}K_{16}(k_{21} + k_{24}).\end{aligned} \tag{A2}$$

When membrane potential is saturating and negative, $k_{21} = k^o_{21}e^{-u}$ is dominant, and terms not containing it drop out of both numerator and denominator. k_{21}, being common to both numerator and denominator, also cancels. Thus, Eq. (5) becomes

$$\frac{I_{K^+}}{-2FN} = \frac{k_{42}K_{16}k_{64}}{K_{16}(k_{42} + k_{46} + k_{64}) + K_{61}(k_{42} + k_{46}) + k_{42}k_{64}} \tag{A3}$$

which can be written in four different ways, to make $[S^+]_o$ or $[D^+]_o$ explicit for either binding order.

With S^+ binding first,

$$\frac{I_{K^+}}{-2FN} = \frac{k_{42}K_{16}k^o_{64}[S^+]_o}{(K_{16} + K_{61})(k_{42} + k_{46}) + (K_{16} + k_{42})k^o_{64}[S^+]_o} \tag{A4}$$

or with S^+ binding last

$$\frac{I_{K^+}}{-2FN} = \frac{k_{64}K_{16}k^o_{42}[S^+]_o}{k_{46}(K_{16} + K_{61}) + K_{16}k_{64} + (K_{16} + K_{61} + k_{64})k^o_{42}[S^+]_o}. \tag{A5}$$

Both expressions have the form of rectangular hyperbolas, or Michaelis functions, in which the Michaelis constant, K_m, is

$$K_m = \frac{(k_{42} + k_{46})(K_{61} + K_{16})}{k^o_{64}(k_{42} + K_{16})} \quad (S^+ \text{ first-on}) \tag{A6a}$$

or

$$K_m = \frac{K_{16}(k_{64} + k_{46}) + K_{61}k_{46}}{k^o_{42}(k_{64} + K_{61} + K_{16})} \quad (S^+ \text{ last-on}). \tag{A6b}$$

Likewise the maximal velocity, I_{max} ($= I_{K^+(max)}$), is given by

$$\frac{I_{max}}{-2FN} = \frac{k_{42}K_{16}}{k_{42} + K_{16}} \quad (S^+ \text{ first-on}) \tag{A7a}$$

or

$$\frac{I_{max}}{-2FN} = \frac{k_{64}K_{16}}{k_{64} + K_{61} + K_{16}} \quad (S^- \text{ last-on}). \tag{A7b}$$

Equations (A6a) and (A7a), with $k^o_{42}[D^+]_o$ substituted for k_{42}, are the expressions given at the top of columns 3 and 4 of Table 1. Equations (A6b) and (A7b), with $k^o_{64}[D^+]$ entered for k_{64}, are in the second section of columns 3 and 4, Table 1.

A similar procedure can be carried out with membrane potential variable, but with one concentration—say $[D^+]_o$—saturating. That leads to

$$\frac{I_{K^+}}{-2FN} = \frac{k_{21}K_{16}k^o_{64}[S^+]_o}{K_{61}(k_{12} + k_{21}) + K_{16}k_{21} + (k_{12} + k_{21} + K_{16})k^o_{64}[S^+]_o} \tag{A8}$$

which is analogous to Eq. (A4) for S^+ binding first; or to

$$\frac{I_{K^+}}{-2FN} = \frac{k_{21}K_{16}k^o_{42}[S^+]_o}{K_{61}(k_{21} + k_{24}) + k_{12}k_{24} + (k_{12} + k_{21} + K_{16})k^o_{42}[S^+]_o} \tag{A9}$$

which is analogous to Eq. (A5) for S^+ binding last. The corresponding expressions for K_m are thus

$$\frac{k_{21}(K_{61} + K_{16}) + k_{12}K_{61}}{k^o_{64}(k_{12} + k_{21} + K_{16})} \quad \text{or} \quad \frac{k_{21}K_{16} + (k_{12} + K_{16})k_{24}}{k^o_{42}(k_{12} + k_{21} + K_{16})} \tag{A10a,b}$$

for S^+ first-on or S^+ last-on, respectively. $I_{max}/(-)2FN$ in this case is the same for both binding orders

$$\frac{k_{21}K_{16}}{k_{12} + k_{21} + K_{16}}. \tag{A11}$$

Again, these expressions, with $k^o_{21}e^{-u}$ substituted for k_{21}, appear in the top two sections of Table 1, columns 1 and 2.

Analogous procedures can be carried out for Models II and III, to give the remaining expressions for K_m and I_{max} listed in Table 1.

Difference Currents

Conditions for reducing the current equations to Michaelian form can be considerably relaxed, at least when K^+ is the primary substrate, by considering the quantity which was actually determined in these experiments, *viz.*, the *I-V* difference current, ΔI_{K^+}. Equation (5) can be rewritten for Model I as

$$\frac{I_{K^+}}{2FN} = \frac{k_{12}k_{24}k_{46}K_{61} - k_{21}K_{16}k_{64}k_{42}}{|\mathbf{M}_4|}. \tag{A12}$$

Now, when $[K^+]_o \to 0$, $k_{64} \to 0$ with K^+ first-on, or $k_{42} \to 0$ with K^+ last-on, and those terms drop out of both the numerator and the denominator. Then the *I-V* difference relationship can be written

$$\frac{\Delta I_{K^+}}{2FN} = \frac{k_{12}k_{24}k_{46}K_{61} - k_{21}K_{16}k_{64}k_{42}}{|\mathbf{M}_4|} - \frac{k_{12}k_{24}k_{46}K_{61}}{|\mathbf{M}_4|^o} \tag{A13}$$

in which $|\mathbf{M}_4|^o$ designates the determinant with $k_{64} = 0$ or $k_{42} = 0$. And this converts to

$$\frac{\Delta I_{K^+}}{-2FN} = \frac{k_{21}K_{16}k_{64}k_{42}|\mathbf{M}_4|^o + k_{12}k_{24}k_{46}K_{61}(|\mathbf{M}_4| - |\mathbf{M}_4|^o)}{|\mathbf{M}_4| \cdot |\mathbf{M}_4|^o} \tag{A14}$$

which is a four-state case of Eq. (11) in Blatt (1986). Without explicitly writing out all the terms, Eq. (A14) can be seen to be of Michaelian form, because (i) $|\mathbf{M}_4| - |\mathbf{M}_4|^o$ has *only* terms containing k_{64} (K^+ first-on; or k_{42}, with K^+ last-on), and (ii) $|\mathbf{M}_4|^o$ has *no* terms containing k_{64} (or k_{42}). Therefore in the numerator of Eq. (A14), all terms contain k_{64} (or k_{42}) *once and only once;* and in the denominator, some terms contain k_{64} (or k_{42}) once, some terms do not contain k_{64} (or k_{42}), and no terms contain k_{64} (or k_{42}) squared.

Obviously, the same argument holds for any single-loop *m*-state model, including the five-state Models II of Fig. 14 and the four-state Models III. But unfortunately it *does not* hold when H^+ is considered the primary substrate, as in the experiments of Figs. 11 and 12, because both numerator and denominator of Eq. (A14) have terms containing the second, first, and zeroth powers of k_{42} (or k_{64}). However, whether or not the general expression for ΔI_{K^+} is Michaelian in form, ΔI_{K^+} becomes so when V_m is large and negative (Figs. 12, 13) or the cosubstrate concentration is saturating (Figs. 10, 11). Then Eq. (A14) gives rise to the same expressions for K_m and I_{max} as have already been written in Table 1 and discussed above.